Materials Today Bio 26 (2024) 101027

Contents lists available at ScienceDirect

Materials Today Bio

journal homepage: www.journals.elsevier.com/materials-today-bio

Magneto-optical nanosystems for tumor multimodal imaging and therapy *in-vivo*

Mengzhen Wang [b], Yin Wang [a,b], Qinrui Fu [a,b,*]

[a] *Key Laboratory of Birth Regulation and Control Technology of National Health Commission of China, Maternal and Child Health Care Hospital of Shandong Province Affiliated to Qingdao University, Qingdao University, Jinan, 250014, China*
[b] *Institute for Translational Medicine, College of Medicine, Qingdao University, Qingdao, 266021, China*

ARTICLE INFO

Keywords:
Magneto-optical nanosystems
Multimodal imaging
Cancer therapy
Precision medicine

ABSTRACT

Multimodal imaging, which combines the strengths of two or more imaging modalities to provide complementary anatomical and molecular information, has emerged as a robust technology for enhancing diagnostic sensitivity and accuracy, as well as improving treatment monitoring. Moreover, the application of multimodal imaging in guiding precision tumor treatment can prevent under- or over-treatment, thereby maximizing the benefits for tumor patients. In recent years, several intriguing magneto-optical nanosystems with both magnetic and optical properties have been developed, leading to significant breakthroughs in the field of multimodal imaging and image-guided tumor therapy. These advancements pave the way for precise tumor medicine. This review summarizes various types of magneto-optical nanosystems developed recently and describes their applications as probes for multimodal imaging and agents for image-guided therapeutic interventions. Finally, future research and development prospects of magneto-optical nanosystems are discussed along with an outlook on their further applications in the biomedical field.

1. Introduction

In recent years, the rapid advancement of nanotechnology has necessitated higher performance standards for nanomaterials [1,2]. Single-component nanomaterials exhibit limitations in terms of single functionality and unstable performance, which significantly impede their further application development. For instance, noble metal nanomaterials with high surface energy are prone to aggregation, resulting in inefficiency and other associated issues. Moreover, single-component nanomaterials often possess only one crucial property that fails to meet multiple requirements simultaneously. Consequently, the emergence of multi-component nanomaterials has garnered considerable attention from researchers due to their ability to combine different components through a robust synergistic coupling effect, thereby offering distinct physical and chemical properties unattainable by single-component nanoparticles [3–6]. Magneto-optical nanosystems are a class of multi-component nanomaterials that are typically fabricated through various methods, including one-pot synthesis, self-assembly techniques, and other approaches. These methods enable the assembly of magnetic nanoparticles and optical materials into structures such as spherical core-shell or core-satellite architectures, heterodimers, multi-component hybrids, vesicle structures, and non-spherical core-shell configurations. This integration effectively combines the magnetic and optical properties to achieve enhanced sensitivity, superior dispersion characteristics, and improved chemical stability compared to single-component nanomaterials by leveraging their intrinsic attributes (e.g., magnetic responsiveness and luminescence) [7–11].

After nearly a decade of extensive development, magneto-optical nanosystems have garnered significant attention owing to their distinctive magnetic and optical properties in diverse applications such as cell separation, fluorescent labeling, disease diagnosis and treatment, biosensing, among others [12–17]. For instance, in comparison to conventional diagnostic and therapeutic nanoagents, magneto-optical nanosystems offer the following advantages: (1) they can serve as imaging agents for multimodal imaging, compensating for the limitations of individual imaging modalities by leveraging the strengths of other modalities to achieve high spatial resolution and accuracy in obtaining

* Corresponding author. Key Laboratory of Birth Regulation and Control Technology of National Health Commission of China, Maternal and Child Health Care Hospital of Shandong Province Affiliated to Qingdao University, Jinan, 250014, China; and Institute for Translational Medicine, College of Medicine, Qingdao University, Qingdao, 266021, China.
E-mail address: fuqinrui2022@qdu.edu.cn (Q. Fu).

https://doi.org/10.1016/j.mtbio.2024.101027
Received 19 January 2024; Received in revised form 11 March 2024; Accepted 13 March 2024

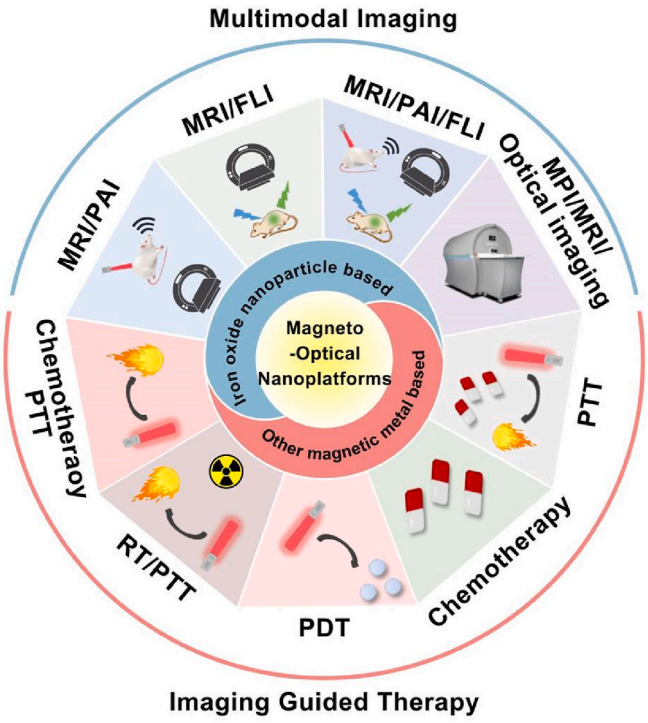

Fig. 1. Schematic illustration of the magneto-optical nanosystems for multimodal imaging and image-guided therapy.

imaging information [18–22]. (2) Apart from passive targeting and accumulation at tumor sites through enhanced permeability and retention (EPR) effect, certain magneto-optical nanosystems can actively target or specifically target disease sites using their magnetic guidance properties along with specific targeting ligands and performance modifiers for drug delivery and imaging purposes [23–29]. (3) Owing to their large surface area or internal loading capacity, some magneto-optical nanosystems can be precisely guided by multimodal imaging techniques for targeted drug delivery and site-specific release at disease locations [30–35]. Based on these inherent advantages, an escalating number of magneto-optical nanosystems have been developed by integrating therapeutic medicine, engineering, and nanotechnology, thereby offering promising prospects for cancer diagnosis and treatment [36–42].

To prevent the aggregation of magnetic nanomaterials and minimize performance loss, magneto-optical nanosystems typically require excellent dispersibility and chemical stability [43–47]. Additionally, these systems should have an appropriate size to pass through capillaries without obstruction in order to avoid ectopic embolism and retention [48–52]. As a result, the development of versatile and applicable magneto-optical nanosystems continues to be a cutting-edge research topic in the field of nanomaterials today [53–55]. This review provides a comprehensive overview of the recent developments in magneto-optical nanosystems and their applications in biomedicine. Firstly, we present a detailed summary and analysis of existing magneto-optical nanosystems, including iron oxide-based platforms as well as those based on other magnetic metals. Subsequently, we focus on the latest advances in multimodal imaging techniques such as magnetic resonance imaging (MRI), magnetic particle imaging (MPI), fluorescence imaging (FLI) and photoacoustic imaging (PAI), all enabled by magneto-optical nanosystems. Finally, we discuss future research directions for these promising technologies (Fig. 1).

2. Magneto-optical nanosystems

The magneto-optical nanosystem comprises MNPs and optical nanomaterials, which exhibit distinct application potentials based on the composition of diverse materials [56–58]. Among these, MNPs typically consist of magnetic elements such as iron (Fe), nickel (Ni), gadolinium (Gd), manganese (Mn), cobalt (Co), and their compounds, offering the advantages of modulating magnetic properties through size and shape variations while facilitating coupling with a range of active groups [24,59–63]. The majority of these MNPs possess inherent ferromagnetic properties and exhibit hysteresis loop characteristics [64,65]. Furthermore, the presence of distinct atomic magnetic moments in different adjacent regions within the MNP gives rise to numerous magnetic domain structures, wherein small spontaneous magnetization regions are formed. This phenomenon determines the size-dependent nature of its magnetic behavior [66]. For example, iron oxide nanoparticles (IONPs) smaller than the single domain limit (approximately 20 nm) exhibit superparamagnetism without magnetic hysteresis at room temperature [67–69]. Moreover, MNPs possess the capability to induce localized magnetic fields, resulting in shortened relaxation times and enhanced proton relaxation within their surrounding environment, thereby potentially influencing MR signal intensity [70–72]. Furthermore, the integration of MNPs and optical nanomaterials can yield synergistic advantages and engender novel applications across diverse fields [73–75]. For instance, magneto-optical nanosystems serve as multi-modal probes that amalgamate the high spatial resolution of MNPs with the heightened sensitivity of optical probes, thereby furnishing more precise complementary information [18,73,76–78]. In subsequent sections, we briefly discuss nanosystems comprising MNPs such as iron oxide, Gd, Ni, Co, and Mn-based nanoparticles in conjunction with a variety of optical materials.

2.1. Iron oxide nanoparticle based composite nanosystem

IONPs are a category of ferromagnetic nanoparticles, which can be categorized into three distinct types: magnetite (Fe_3O_4), maghemite (γ-Fe_2O_3), and mixed ferrite (MFe_2O_4) [79]. Due to their exceptional properties such as biocompatibility and relativity, extensive research has been conducted on IONPs in the fields of biomedicine and bioengineering [30,80–84]. When the size of IONPs is smaller than the critical threshold (*e.g.*, when the diameter of spherical magnetite NPs is less than approximately 20 nm), superparamagnetism can be observed in these IONPs at room temperature [85–87]. The superparamagnetic iron oxide nanoparticles (SPION) exhibit a high magnetic moment in the presence of an external magnetic field, while demonstrating no hysteresis phenomenon with zero remanence and coercivity (*Hc*) after the withdrawal of the magnetic field. This ensures the maintenance of colloidal stability even under zero magnetic fields, thereby preventing agglomeration [88–90]. In recent years, multifunctional nanosystems composed of IONPs and various optical nanomaterials have received a lot of attention in advancing clinical diagnostics and therapeutics due to their special magnetic and optical properties [61,91]. In this section, we briefly introduce different types of optical nanomaterials, mainly including inorganic nanomaterials and organic fluorescent dyes, with IONPs to compose different magneto-optical nanosystems.

Inorganic optical nanomaterials such as semiconductor quantum dots (QDs), carbon-based nanomaterials, graphene, lanthanide-doped nanomaterials, and plasmonic nanomaterials offer a range of advantages for tumor diagnostic and therapeutic applications, including stability, excellent fluorescence and photoacoustic (PA) properties, and high antioxidant properties. These advantages make them uniquely valuable in the diagnosis and treatment of disease and provide strong support for the advancement of clinical medicine. In recent years, semiconductor nanomaterials such as QDs have garnered significant attention due to their wide excitation absorption range, narrow and symmetric light emission, strong luminescence, and excellent photostability [92,93]. QDs are semiconductor nanoparticles with a diameter ranging from 2 to 10 nm, composed of group II-VI or III-V elements (such as CdSe and CdTe). They exhibit excellent photoluminescence (PL)

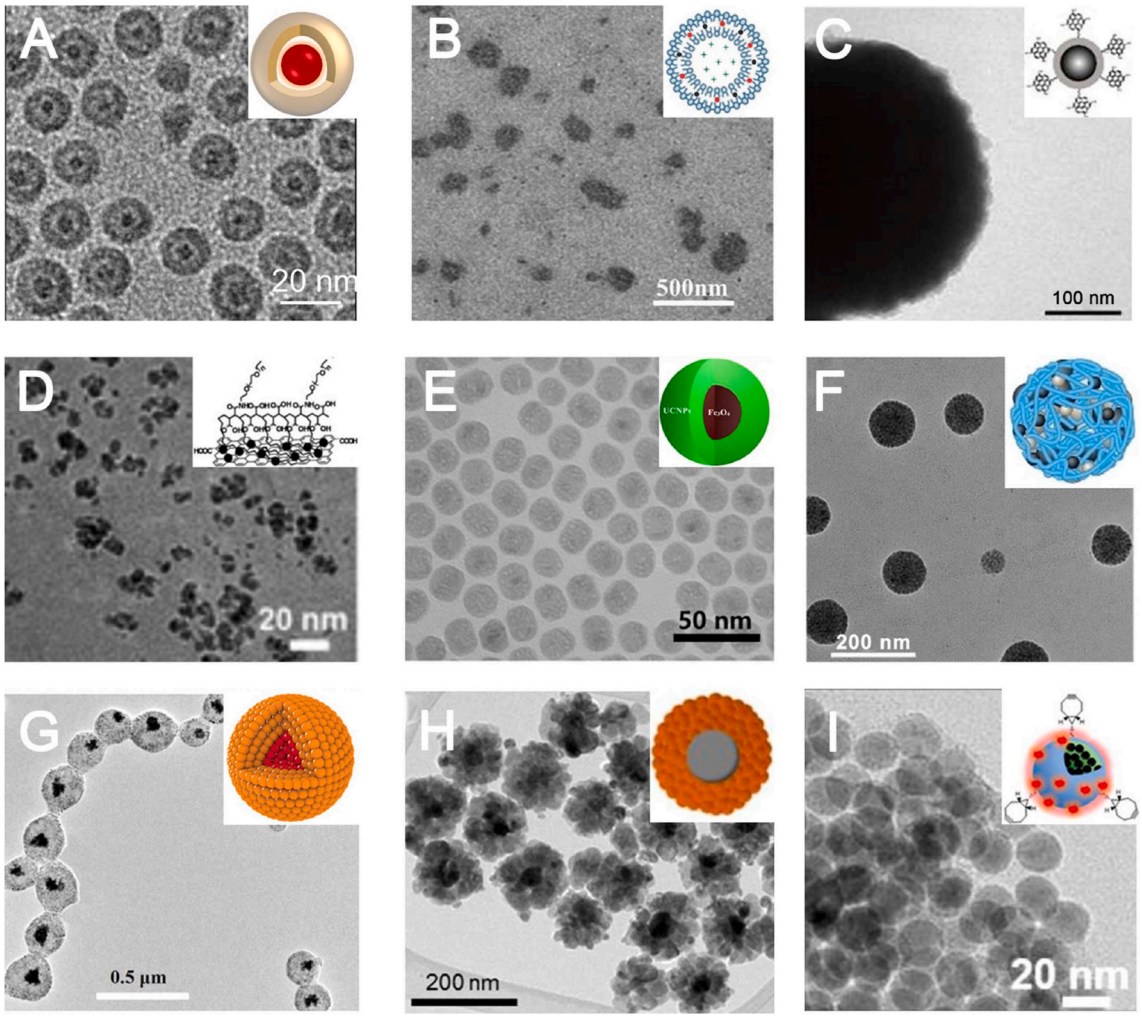

Fig. 2. Transmission electron microscope (TEM) images of QD@MHS NPs, QSC-Lip, HMNS/SiO_2/GQD, RGO-IONP-PEG, Fe@UCNPs, IO/DCNP@PP NPs, MPNAs, Ag/Fe_3O_4 NFs, BCN-dual-NPs-20. [(A) reproduced with permission from Ref. [98], Copyright 2020, Elsevier. (B) reproduced with permission from Ref. [99], Copyright 2018, Wiley-VCH GmbH. (C) reproduced with permission from Ref. [109], Copyright 2016, Ivyspring International. (D) reproduced with permission from Ref. [116], Copyright 2012, Wiley-VCH GmbH. (E) reproduced with permission from Ref. [126], Copyright 2019, Elsevier. (F) reproduced with permission from Ref. [127], Copyright 2022, Wiley-VCH GmbH. (G) reproduced with permission from Ref. [134], Copyright 2019, Wiley-VCH GmbH. (H) reproduced with permission from Ref. [137], Copyright 2016, American Chemical Society. (I) reproduced with permission from Ref. [148], Copyright 2019, American Chemical Society].

properties [94]. By combining QDs with IONPs, magneto-optical nanosystems can be formed, which possess stable collective luminescence and magnetic properties for *in vitro* and *in vivo* biological imaging and therapy [95–97]. For example, The QDs-iron oxide composite nanosystems with core-hollow shells can effectively mitigate the degradation of optical properties induced by the interaction between QDs and MNPs. Park et al. synthesized magnetic Fe_2O_3 hollow sphere nanoparticles encapsulated with CdSeTeS QDs (QD@MHS NPs), which exhibited both magnetic and fluorescent properties (Fig. 2A) [98]. The hollow structure of QD@MHS NPs demonstrated the advantage of a gap between the Fe_2O_3 shell and the QDs core, promoting fluorescence generation by limiting charge and energy transfer between substances and preventing fluorescence quenching. Furthermore, co-encapsulation of IONPs and QDs in polymer or organic materials effectively avoided non-specific distribution *in vivo* and potential toxic effects, enabling the formation of multifunctional magneto-optical nanosystems. Zhao et al. developed a theranostic nanosystem (QSC-Lip) with magnetic targeting (MT) function by collectively encapsulating QDs, SPIONs, and cilengitide into PEGylated liposomes. This platform accurately guided surgical resection of glioma through dual-imaging techniques (MRI and FLI) (Fig. 2B) [99].

Carbon-based nanomaterials, such as carbon dots (CDs), carbon nanotubes and graphene-based nanomaterials can be combined with IONPs to form nanosystems with magnetic and optical properties for biomedicine [100]. CDs, a new focus in carbon-based nanomaterials, mainly include three types: graphene quantum dots (GQDs), carbon quantum dots, and carbonized polymer dot [101,102]. Due to the presence of surface functional groups, π-conjugated domains, carbon-oxygen and carbon-nitrogen double bonds, CDs exhibit exceptional light absorption properties, tunable PL characteristics, high quantum yield (QY), photostability, and efficient reactive oxygen species (ROS) scavenging ability [103–105]. Consequently, by combining with IONPs, magneto-optical nanosystems with reduced cytotoxicity can be fabricated for diverse biomedical applications [106,107]. For example, Dhara et al. successfully synthesized composite nanoparticles (FeCD) of CDs doped with SPION using a facile hydrothermal method, exhibiting exceptional magnetic properties, fluorescence characteristics, and biocompatibility [108]. Furthermore, GQDs can be conjugated with silica-coated IONPs to create multifunctional nanosystems. For instance, Liu et al. achieved the synergistic effect of magneto-mechanical and photothermal stimulation by employing a condensation reaction between amino and carboxyl groups to combine carboxylated GQDs with hollow magnetic nanospheres (HMNSs) composed of Fe_3O_4 coated with an amino-functionalized silica shell (HMNS/SiO_2/GQDs) (Fig. 2C) [109].

Graphene, serving as the fundamental constituent of all other carbon-based materials, comprises a monolayer of sp^2 carbon atoms arranged in a hexagonal lattice structure. This unique configuration offers notable advantages including an expanded surface area, facile functionalization and enhanced solubility, as well as heightened absorbance capabilities [110,111]. The combination of graphene and MNPs was achieved through two structures: encapsulation of MNPs within graphene-based materials, and decoration of graphene-based materials with MNPs [112]. Among these structures, the decoration of graphene-based materials with MNPs is widely employed [113,114]. However, in this structure, the lack of protection for the MNPs necessitates loading additional functionalized substances such as polyethylene glycol (PEG) and chitosan [115]. For instance, Liu et al. synthesized reduced graphene oxide (RGO) nanosheets containing IONPs *via* a hydrothermal reaction and subsequently modified them with PEG to fabricate an innovative probe (RGO-IONP-PEG) for cancer imaging and therapy **(**Fig. 2D**)** [116].

Lanthanide-doped nanoparticles have garnered sustained attention in the biomedical field owing to their tunable emission characteristics, minimal photobleaching, exceptional photostability, and prolonged PL lifetime [117–119]. Typically, they exhibit near-infrared fluorescence (NIRF) upon excitation with NIR light *via* either upconversion (UC) or downconversion (DC) pathways, thereby classifying them into upconversion nanoparticles (UCNPs) and downconversion nanoparticles (DCNPs) [120]. UCNPs are a class of innovative fluorescent nanomaterials consisting of three components: a sensitizer (*e.g.*, Yb^{3+}), emitters (*e.g.*, Tm^{3+}, Er^{3+}, Ho^{3+}), and a host matrix. These materials exhibit an anti-Stokes process, wherein they absorb two or more low-energy photons and emit one high-energy photon [121–124]. The integration of UCNPs with iron oxide composite nanosystems not only combines the advantages of UCNPs, such as light stability, deep light penetration, and minimal background interference but also enhances their upconversion luminescence (UCL) efficiency *in vivo*, thereby overcoming the limitations associated with biological imaging and clinical applications [125]. Li et al. prepared multifunctional nanosystems with core-shell structure (Fe@UCNP@HMME), consisting of Fe_3O_4 core, $NaGdF_4$:Yb:Er (UCNPs) shell and hematoporphyrin monomethyl ether (HMME). These nanosystems exhibited excellent luminescence properties with UCL bands and superparamagnetic properties **(**Fig. 2E**)** [126]. The optical properties of DCNPs are enhanced by the downconversion luminescence mechanism, which follows the PL phenomenon of Stokes law. This enables the formation of magneto-optical nanosystems with IONPs for diverse applications in the biomedical field. Fu et al. developed a nanocomposite (IO/DCNP@PP) consisting of a hybrid assembly of pheophorbide-A (PP)-modified IONPs and lanthanide-doped DCNP, resulting in magnetic nanochains exhibiting T_2-MRI and FLI characteristics for cancer therapy (Fig. 2F) [127].

Plasma nanomaterials, such as gold, silver, and platinum nanoparticles, exhibit unique localized surface plasmon resonance (LSPR) effects that result in their exceptional light absorption and scattering capabilities when exposed to incident light [128–130]. The iron oxide-plasma composite nanosystems, featuring diverse structures, have garnered significant attention among researchers due to their possession of both the magnetic properties of IONPs and the optical properties of plasma nanoparticles. Gold nanomaterials, including spherical nanoparticles (AuNPs), nanorod, and nanoshell, possess distinctive attributes such as photodegradation, photothermal effects, exceptional biocompatibility, precise size control, X-ray absorption capability. When integrated with IONP, they can form versatile nanosystems with diverse architectures [128,131]. The iron oxide-Au nanosystem with a core-shell structure is currently the most extensively investigated type, encompassing two predominant forms: one with an iron oxide core and the other with a gold core. Research has demonstrated that incorporating gold nanoshells can effectively prevent aggregation, oxidation, and corrosion of IONPs while simultaneously enhancing surface functionalization and chemical stability in the core-shell nanosystems [132]. Wang et al. employed Ag-coated SPION (SPIO–Ag) as a template for the synthesis of SPIO-hollow gold nanoshells (SPIO-HGNs) *via* a single displacement reaction, resulting in tunable inner diameter, NIR LSPR peak, and magnetic properties [133]. Incorporating IONP as the shell and gold as the core, an alternative core-shell structure is devised to seamlessly integrate magnetic and plasma components within single nanosystems, effectively circumventing the magnetic shielding effect of gold nanoshells for achieving optimal saturation magnetization and plasma optical activity. Chen et al. employed a self-assembly strategy to coassemble oleic acid-coated IONPs (OC-IONPs) and oleylamine-coated gold nanoparticles (OA-AuNPs), resulting in the formation of colloidal magnetic-plasma nanoassemblies (MPNAs) with core-shell heterostructures, which exhibited exceptional preservation of their magnetic-plasma activity (Fig. 2G) [134].

In addition to iron oxide-Au nanosystems, another composite nanosystem comprising Ag and IONPs with both plasmonic and magnetic properties exhibits significant potential for imaging and therapy [135]. Due to the LSPR characteristic of Ag nanomaterials, namely, the oscillation of conduction electrons at the surface leading to enhanced energy absorption and temperature increase upon excitation by incident light, Ag nanomaterials typically exhibit a pronounced photothermal effect [136]. Therefore, the iron oxide-Ag composite nanosystems can synergistically harness the magnetic heating effect of MNPs induced by hysteresis loss (Néel and Brown relaxation) and the photothermal effect of plasma Ag to efficiently execute cancer hyperthermia. The magnetic silver/magnetite (Ag/Fe_3O_4) nanoflowers (NFs) were fabricated by Srikanth et al. through a one-step solvothermal process, where clustered Fe_3O_4 nanoparticles acted as petals surrounding silver cores. These NFs demonstrated exceptional magnetic and photothermal properties (Fig. 2H) [137].

However, inorganic nanomaterials usually suffer from the problem of slow excretion after administration and tend to linger in the major organs of the reticuloendothelial system, which may lead to long-term toxicity. Organic semiconductor materials such as organic fluorescent dyes, which are completely benign and biologically inert, avoid this toxicity problem. Organic fluorescent dyes typically possess extensive conjugated systems, such as multiple aromatic rings or carbon-carbon double bonds [138,139], enabling them to emit longer-wavelength light upon excitation at a specific wavelength [140–142]. These dyes exhibit excellent biocompatibility, high molar absorption coefficients, and superior fluorescence QY [143–145]. By incorporating organic fluorescent dyes into composite nanosystems through coupling or embedding with lipid- or silica-coated shells on the surface of IONP cores, enhanced versatility is achieved, thereby demonstrating significant practical value in diverse fields including biosensing, laboratory analysis, and clinical diagnosis [146,147]. For example, Kim et al. developed nanoparticles (BCN-dual-NPs) with dual-modality FLI and MRI. These nanoparticles were formed by chemically coupling a NIRF dye Cy5.5 with bicyclo [6.1.0]nonyne (BCN)-conjugated glycol chitosan nanoparticles (BCN-NPs), followed by packaging oleic acid-coated SPIONs (OA-Fe_3O_4 NPs) within the BCN-NPs [148]. This innovative design enabled non-invasive and precise stem cell tracking through high-intensity NIRF and T_2-weighted MR signal acquisition (Fig. 2I). Additionally, the BCN-dual-NPs exhibited enhanced local magnetic dosage as a result of the aggregation of 20 nm OA-Fe_3O_4 NPs within the BCN-dual-NPs, leading to the formation of high-density ion clusters.

2.2. Alternative nanosystems based on magnetic metals composites

Gd, a paramagnetic lanthanide metallic element, possesses a distinctive 4f electron cloud structure characterized by the presence of seven unpaired electrons. The spins of these electrons can generate substantial magnetic moments that significantly impact the magnetic relaxation of water protons [149,150]. Therefore, the strong paramagnetic properties and high magnetic moment of Gd make it a promising candidate for MRI contrast agents [151]. The presence of Gd can

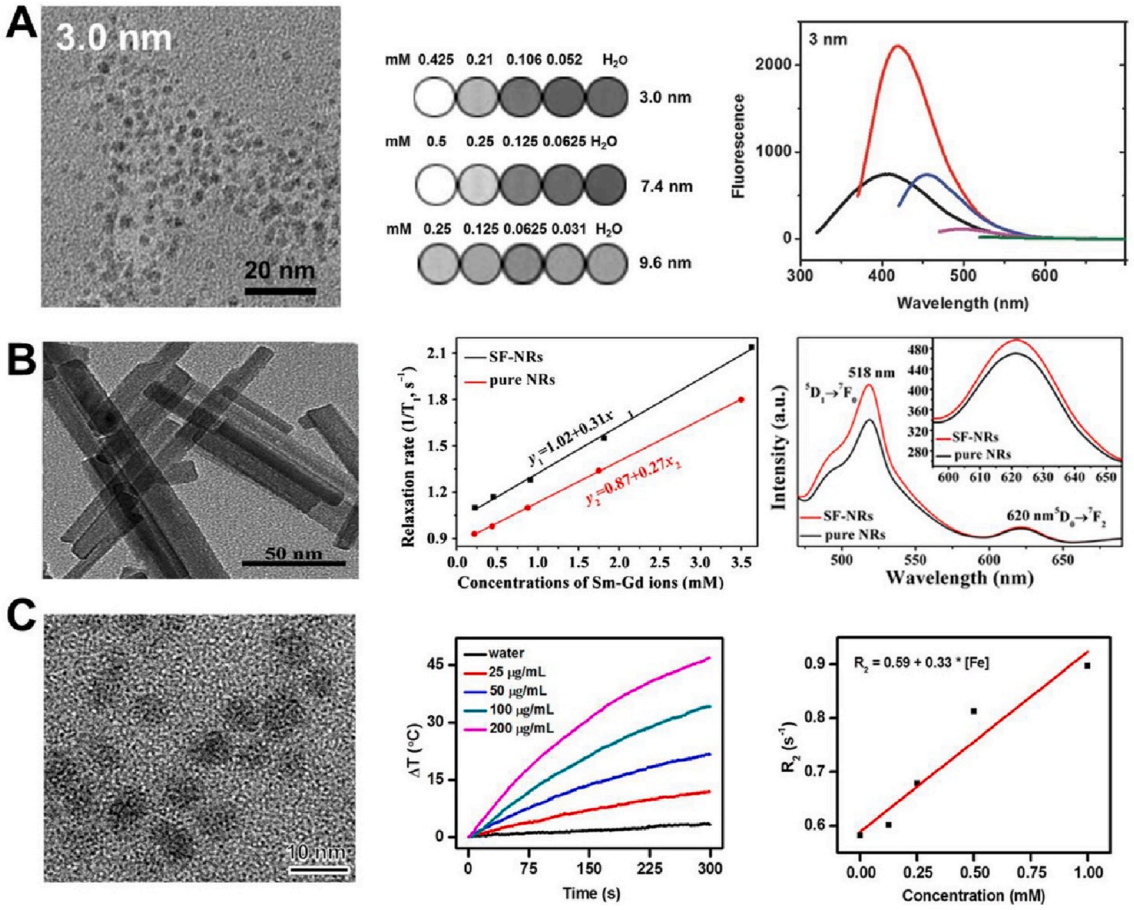

Fig. 3. (A) TEM image of Gd@C-dots, T_1-weighted MR Images, and PL spectra at different wavelengths of excitation. (B) TEM image, the plot of relativity ($1/T_1 = r_1$) and emission spectrum of SF-NRs. (C) TEM image of $CuFeSe_2$ NCs, heating curves of pure water and aqueous dispersions of $CuFeSe_2$ NCs at different concentrations under laser irradiation, and transverse relativity (r_2). [(A) reproduced with permission from Ref. [156], Copyright 2016, Wiley-VCH GmbH. (B) reproduced with permission from Ref. [157], Copyright 2015, Elsevier. (C) reproduced with permission from Ref. [164], Copyright 2017, American Chemical Society].

induce significant fluctuations in the magnetic field, leading to a reduction in spin-lattice longitudinal relaxation time (T_1) and consequently enhancing the brightness of T_1-weighted images [152–154]. Incorporation of Gd species into diverse nanostructures, including QDs, copper chalcogenide nanocrystals (NCs), and other lanthanide nanostructures, enables the formation of multifunctional magneto-optical nanosystems as multimodal probes, exhibiting significant research potential in the biomedical domain [155]. For example, synthesized size-controlled Gd-encapsulated carbonaceous dots (Gd@C-dots) using a mesoporous silica nanoparticle-templated method, which exhibited magnetic and optical properties dependent on their sizes [156]. The smallest Gd@C-dots demonstrated the highest longitudinal relativity (r_1 = 10 mM^{-1} s^{-1}) and fluorescence QY (30.2%) (Fig. 3A). In addition to their exceptional magnetic properties, Ln^{3+} ions also exhibit well-defined energy levels spanning from UV to visible and infrared regions due to the effective shielding of the 4f orbital by the occupied 5s and 5p orbitals. This results in tunable emission characteristics, minimal photobleaching, outstanding photostability, and prolonged PL lifetime of lanthanum-doped nanostructures. Consequently, various nanosystems co-doped with lanthanides such as Gd and Europium (Eu) have been developed and demonstrated remarkable magnetic and optical properties for multifunctional biomedical applications. For example, Gao et al. employed a feasible biomineralization process to synthesize silk fibroin (SF) peptide-coated $SmPO_4$ nanorods (SF-NRs) co-doped with Gd and Eu, which exhibited paramagnetic and photoluminescent properties and demonstrated enhanced r_1 relativity compared to the SF-NRs doped solely with a single lanthanide ion (Fig. 3B) [157].

Moreover, Copper chalcogenides NCs, a category of nanoscale transition metal chalcogenides, exhibit distinctive optical and magnetic properties and can be effectively integrated with other substances such as Gd^{3+} to construct multifunctional magneto-optical nanosystems [158,159]. The binary copper sulfur compounds, characterized by the rigid crystal framework formed by sulfur atoms and the random occupation of copper atoms in the lattice of sulfur atoms, readily give rise to copper defects ($Cu_{2-x}E$ (x = 0, 1; E = S, Se, Te)) [160,161]. Due to the presence of Cu vacancies, the population of free carriers in NCs increases, thereby inducing LSPR, which exhibits a broad absorption band in the NIR region and effectively facilitates the conversion of NIR light into thermal energy [162]. For example, Zhang et al. developed a biocompatible Gd-integrated CuS nanotheranostic agent, Gd:CuS@BSA, using bovine serum albumin (BSA) as a biotemplate through a biomimetic approach [163]. This agent demonstrated exceptional photothermal conversion efficiency, robust PA signals, and suitable longitudinal relativity (r_1 = 16.032 mM^{-1} s^{-1}). Moreover, copper deficiency induces paramagnetism in copper chalcogenide NCs and offers opportunities for their versatility and customization. For instance, magnetic elements such as Fe, Ni, Co, Mn can be incorporated into copper chalcogenides to form ternary or quaternary compounds with magnetic and optical properties that exhibit promising prospects for practical applications. For example, the ultrasmall magnetic $CuFeSe_2$ ternary NCs (<5.0 nm) were synthesized by Li et al. using an environmentally friendly aqueous method, demonstrating exceptional superparamagnetism, broad NIR absorption in the 500–1100 nm range, and a high photothermal conversion efficiency of 82%. These NCs hold great

Table 1
A comprehensive overview of the diagnostic applications, strengths, and limitations of magneto-optical nano-systems in various imaging diagnostics.

Magneto-optical nanosystems	Diagnostic application	Strengths	Limitations	Ref
RGD-RFP-LBT-Gd	MRI/FLI	Bimodal MRI/FLI integrates MRI and FLI to address the inherent limitations of each modality, namely the reduced sensitivity of MRI and limited tissue penetration of FLI in deep-seated tumors.	Under physiological conditions, the fluorescence intensity of FLI/MRI bimodal probes is usually affected by aggregation-induced bursting effects.	[174]]
P-CyFF-Gd				[176]
JVs	MRI/PAI	The magneto-optical nano-system, which integrates PAI and MRI, possesses the complementary advantages of exceptional optical contrast, high spatial and temporal resolution, as well as soft tissue resolution. Consequently, it achieves a synergistic imaging effect that surpasses the sum of its individual components.	Most magneto-optical nanosystems for MRI/PAI suffer from relatively poor biocompatibility, the need for large doses of nanoscale agents, inadequate targeting, suboptimal tissue biodistribution, lack of proper assessment of pharmacokinetics, and difficulty in accurate quantification.	[182]
CP-IO				[183]
CS_2-ICG	MRI/FLI/PAI	The combined MRI/FLI/PAI magneto-optical nanosystem enables real-time whole-body scanning with fluorescence imaging to localize the location of surface tumors, high-resolution whole-body scanning with MRI to precisely identify anatomical structures and locate deeper tumors, and PAI to obtain a heterogeneous distribution of the contrast agent within the tumor.	The majority of magneto-optical nanosystems for MRI/PAI/FLI are still in the proof-of-concept stage and necessitate extensive trials to validate their efficacy and clinical applicability.	[186]
cRGD-CM-CPIO				[188]
TSP NPs	MPI/MRI/FMI	The sensitivity of MPI is exceptionally high, and it can be complemented with MRI and optical imaging to achieve superior spatial resolution. This combination enables real-time visualization of anatomical details, as well as *in vivo* assessment of distribution and clearance processes.	The development of MPI is still in its nascent stages and necessitates further advancements in imaging hardware, alongside the establishment of its clinical feasibility.	[193]
MMPF NP	MPI/MRI/FLI/PAI			[195]

potential for multimodal imaging-guided photothermal therapy (PTT) (Fig. 3C) [164].

3. Magneto-optical nanosystems for multimodal imaging

Multimodal imaging, integrating two or more imaging modalities, has emerged as a robust tool for precise disease diagnosis and comprehensive analysis of disease progression in both basic biomedical research and clinical settings [165,166]. In the aforementioned section, we have summarized that magneto-optical nanosystems possess exceptional magnetic and optical properties owing to their amalgamation of diverse magnetic and optical nanomaterials. These magneto-optical nanosystems hold significant potential for applications in the biomedical field, particularly in imaging, where they surmount the limitations of single imaging techniques by enabling non-invasive imaging with enhanced penetration depth, resolution, and sensitivity [23]. In the subsequent section, our focus will be on the utilization of magneto-optical nanosystems for multimodal imaging (Table 1).

3.1. Dual-modality MRI/optical imaging

3.1.1. Dual-modality MRI/FLI

In dual-modality MRI/FLI, while MRI provides three dimensional (3D) anatomical images with high spatial resolution and wireless tissue penetration depth that FLI cannot offer [167,168], FLI can provide real-time and highly sensitive biochemical information that is lacking in MRI [169]. MRI involves exciting the nucleus of a proton using a radio frequency pulse under an external magnetic field generated by an MRI scanner, followed by processing the released radio signals from the proton's nucleus after cessation of the radio frequency pulse. Magneto-optical nanosystems can serve as contrast agents in MRI by generating localized magnetic fields that interfere with the nuclear relaxation of surrounding magnetic nuclei, thereby enhancing signal contrast between the background and adjacent regions in MR images. This is achieved through acceleration of nearby protons' relaxation process and shortening of their spin-lattice longitudinal relaxation time (T_1) or spin-spin transverse relaxation time (T_2) [170,171]. Specifically, magneto-optical nanosystems function as T_1-type contrast agents when r_2/r_1 ratio falls within 1–5, resulting in brightened T_1-weighted imaging; whereas for r_2/r_1 values exceeding 10, they act as T_2-type contrast agents leading to darkened T_2-weighted imaging [172,173]. Additionally, magneto-optical nanosystems exhibit distinctive luminescence features that make them suitable for use as FLI contrast agents. In recent years, there has been significant interest in magneto-optical nanosystems that integrate FLI and MRI, as they capitalize on the complementary advantages offered by these two imaging modalities.

The magneto-optical nanosystems possess excellent biocompatibility and exhibit target site-specific accumulation, making them highly effective as a dual-mode MRI/FLI probe. Yang et al. developed a

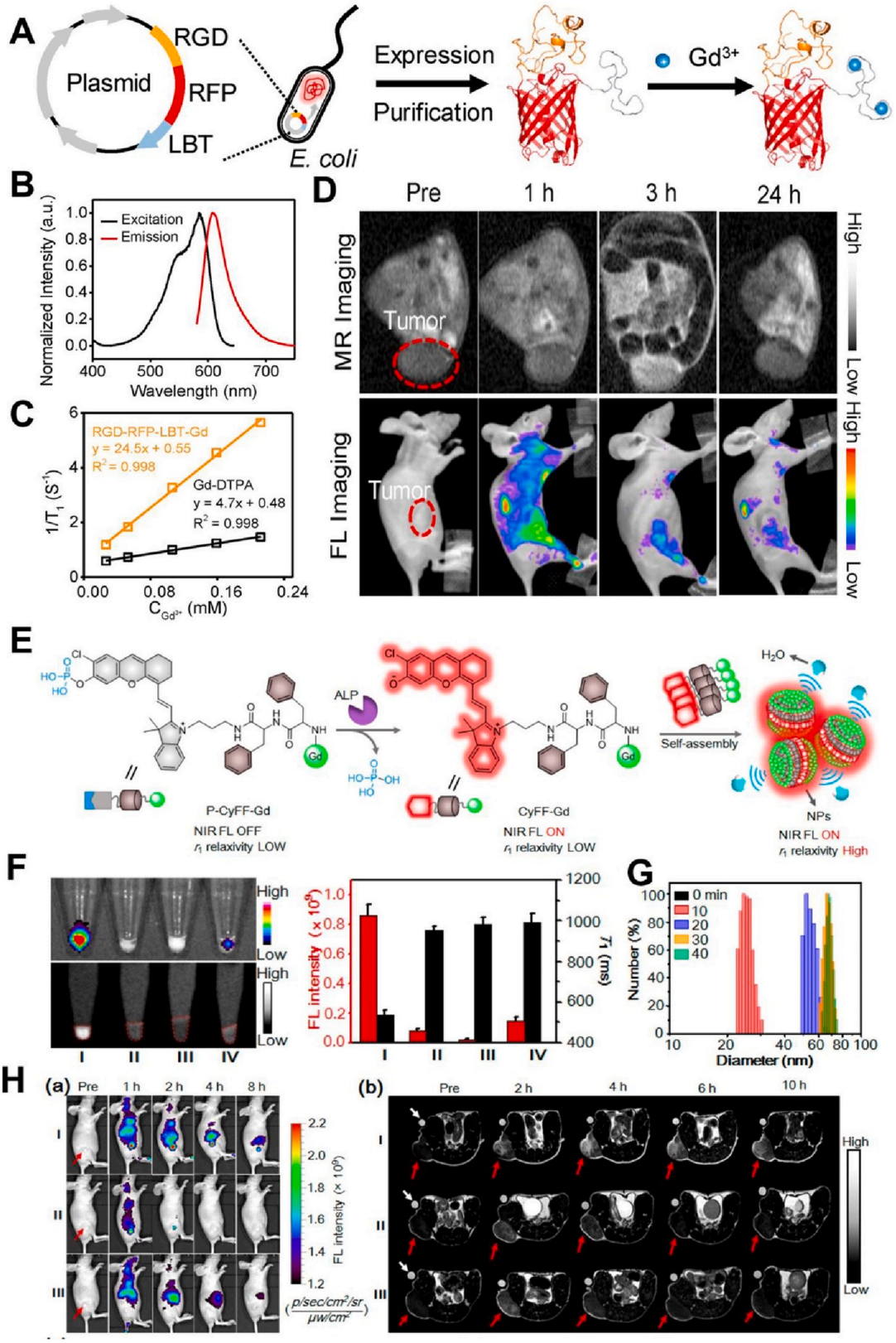

Fig. 4. (A) Schematic representation of the preparation process of RGD-RFP-LBT-Gd. (B) Fluorescence emission and excitation spectra of RGD-RFP-LBT-Gd. (C) Plots of r_2 value of RGD-RFP-LBT-Gd and Gd-DTPA. (D) Enhanced MR and FL images of tumor-bearing mice at different time points after RGD-RFP-LBT-Gd injection. (E) Schematic of the in situ self-assembly and activation of P-CyFF-Gd. (F) FL and T_1-weight MR imaging of P-CyFF-Gd incubated HeLa cells with the change of FL intensity and T_1 value. (G) After incubation with ALP (2U/mL) at 37 °C, the size change of P-CyFF-Gd (200 μM) over time by DLS. (H) FL imaging (a) and T_1-weighted MR images (b) of mices receiving i. v. injection of P-CyFF-Gd (I), P-Cy-Gd (II), or P-CyFF-Gd (50 μM, 200 μL) together with i. t. injection of 10 mM Na_3VO_4 (50 μL) (III). [(A)–(D) reproduced with permission from Ref. [174], Copyright 2020, Elsevier. (E)–(H) reproduced with permission from Ref. [176], Copyright 2021, American Chemical Society].

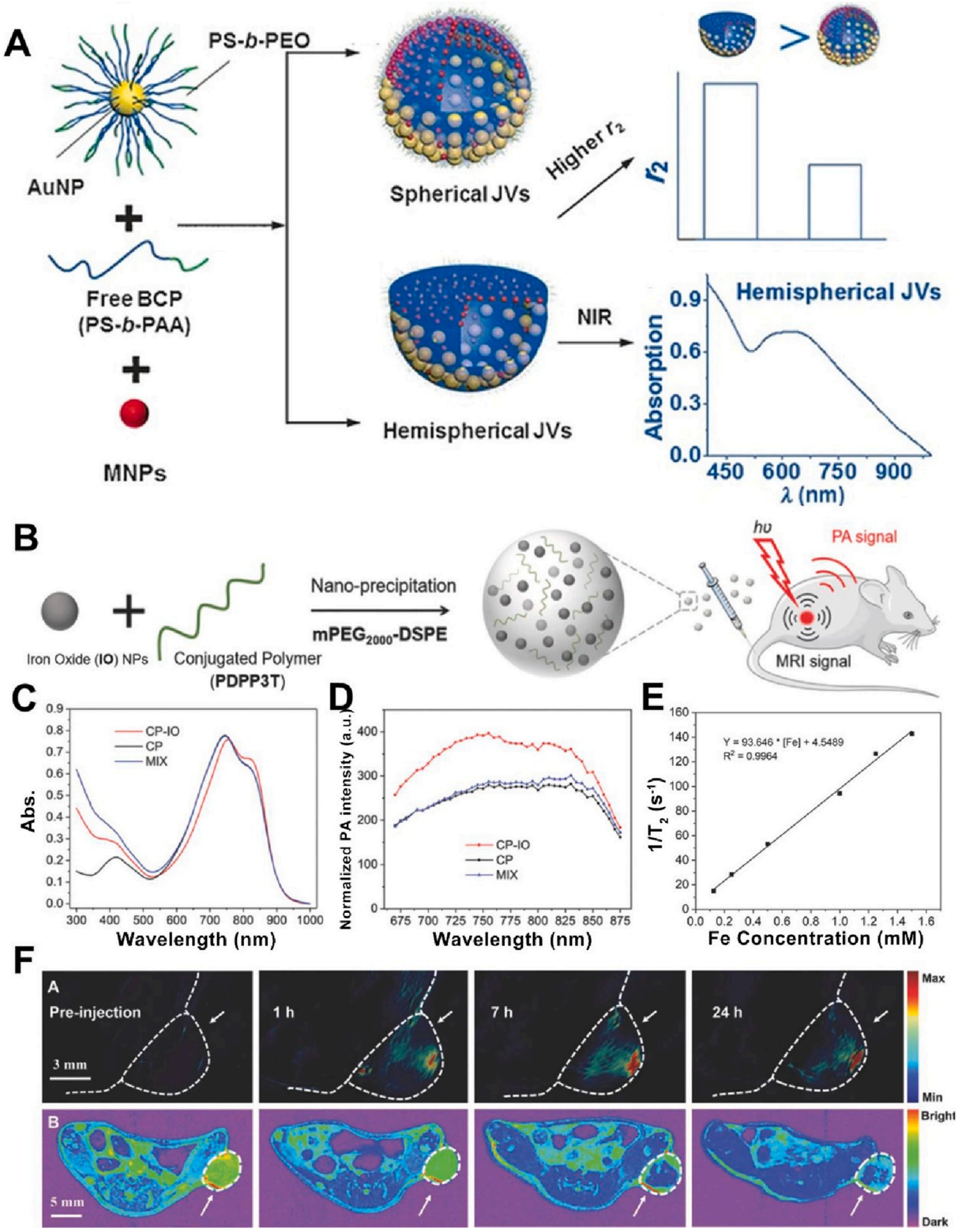

Fig. 5. (A) Preparation of hemispherical and spherical JVs and their r_2 relativity and NIR absorption. (B) The preparation process of CP-IO. Absorption spectra (C), PA spectra (D) of CP-IO at a CP concentration of 0.03 mg mL^{-1}. (E) The plot of relativity ($1/T_2 = r_2$). (F) *In vivo* PA images and T_2-weighted MR images of mice treated with CP-IO. [(A) reproduced with permission from Ref. [182], Copyright 2016, Wiley-VCH GmbH. (B)–(F) reproduced with permission from Ref. [183], Copyright 2018, Wiley-VCH GmbH].

biosynthetic approach to fabricate a functional protein-based probe (RGD-RFP-LBT-Gd) comprising an Arg-Gly-Asp (RGD) peptide, red fluorescence protein (RFP), and lanthanide-binding tag (LBT) with Gd. This probe demonstrated remarkable RGD-mediated tumor targeting ability, enabling sensitive dual-mode FLI/MRI imaging with exceptional spatial resolution (Fig. 4A) [174]. Due to the red fluorescence emission characteristic of RFP and its unique barrel structure, RGD-RFP-LBT-Gd exhibited pH-stable fluorescence emission at 607 nm (Fig. 4B). the

incorporation of highly paramagnetic Gd^{3+} into RGD-RFP-LBT resulted in excellent MR Imaging performance with high r_1 of 24.5 mM^{-1} s^{-1} (Fig. 4C). The experiment co-incubated U87MG cells with RGD-RFP-LBT-Gd demonstrated specific absorption and accumulation of RGD-RFP-LBT-Gd by tumor cells due to the specific binding ability of the RGD domain to αvβ3 integrin receptor, which is up-regulated on the surface of tumor cells. Compared to the RPF treatment group, RGD-RFP-LBT-Gd exhibited a stronger fluorescence signal. *In vivo* imaging results revealed a significant increase in FLI and MRI signals at tumor sites after injecting RGD-RFP-LBT-Gd, providing additional complementary information for tumor diagnosis (Fig. 4D). Furthermore, no apparent injuries or lesions were observed in the organs of treated mice, indicating excellent biocompatibility of RGD-RFP-LBT-Gd and its potential for further *in vivo* imaging applications.

However, multimodal imaging probes with "always on" imaging signals may encounter challenges in achieving a high signal-background ratio (SBR). Consequently, recent advancements have led to the development of dual-mode MRI/FLI nanosystems that possess biomarker response activation capabilities, effectively mitigating background signals and enhancing SBR for real-time *in vivo* imaging [175]. For example, Ye et al. developed bimodal probes (P-CyFF-Gd) for *in vivo* tumor imaging by combining alkaline phosphatase (ALP)-activatable NIR fluorescence and MRI techniques [176]. These probes were designed with a prequenched NIR fluorophore (merocyanine, Cy-Cl) caged by a phosphate group (-PO_3H), a paramagnetic DOTA-Gd chelate, and a hydrophobic dipeptide Phe-Phe (FF) linker (Fig. 4E). Originally, P-CyFF-Gd was a water-soluble small molecule probe with characteristics of NIR fluorescence and low r_1 relativity (8.9 ± 0.3 mM^{-1} s^{-1} at 0.5 T). Its small size and hydrophilicity facilitated its entry into tumor tissues. Upon diffusion into ALP-positive tumor tissues, P-CyFF-Gd underwent an ALP-triggered fluorescence reaction to release CyFF-Gd, which exhibited activated NIR fluorescence emission at 710 nm (Fig. 4F). Subsequently, the self-assembly of CyFF-Gd occurred through intermolecular interactions mediated by its FF dipeptide moiety, resulting in the formation of magneto-optical nanoparticles with larger sizes that limited molecular rotation and prolonged the tumbling time (τR) of the DOTA-Gd chelate. This led to an increased r_1 relativity value of 20.1 ± 0.5 mM^{-1} s^{-1} (Fig. 4E and F). Furthermore, the self-assembled nanoparticle was found to accumulate in tumor lysosomes by endocytosis due to its ability to easily anchor to cell membranes. This accumulation further increased tumor NIR fluorescence and MR contrast. In vivo imaging results revealed a gradual enhancement of tumor fluorescence and T_1-weighted MR contrast in HeLa-tumor-bearing mice following the intravenous injection of P-CyFF-Gd, with the maximum signal enhancement (%SE) reaching approximately 2.8-fold higher than that of the control group without aggregation (P-Cy-Gd treatment) at 4 h (Fig. 4H). The significantly enhanced MRI/FLI results not only helped to identify and map the edges of the orthotopic liver tumors, but also enabled image-guided surgical excision, establishing a solid foundation for further design and application.

In summary, magneto-optical nanosystems with MRI/FLI capabilities have great potential for application in precise localization of tumors. Secondly, some magneto-optical nanosystems have also been investigated for monitoring the treatment of tumors. For example, Song et al. investigated a DNA-functionalized ultrasmall IONPs self-assembled to form an imaging and therapeutic platform that can provide a switchable MRI/dual-channel fluorescence signal to monitor the process of adaptive ferroptosis therapy [177].

3.1.2. Dual-modality MRI/PAI

In the context of dual modality MRI/PAI, MRI enables multi-directional imaging of diseased regions and provides high spatial resolution information for precise identification of specific pathological locations; PAI with high sensitivity facilitates rapid real-time scanning, thereby enabling dynamic visualization based on MRI [178,179]. The MR-PAI bimodal contrast agent, utilizing magneto-optical nanosystems, can be employed for both MRI and PAI. It modulates relativity for enhanced MRI performance and converts light energy into thermal energy to generate ultrasonic signals for PAI [180]. For instance, magneto-optical nanosystems incorporating PA contrast agents such as AuNPs or conjugated polymers (CPs) are capable of absorbing pulsed laser light energy and converting it into heat, resulting in thermoelastic expansion followed by ultrasonic emission that can be captured by an ultrasound transducer and reconstructed into PA images [181]. Nie et al. successfully developed hemispherical magneto-plasmonic Janus vesicles (JVs) by combining hydrophobic Fe_3O_4-MNPs, an amphiphilic block copolyme composed of polystyrene-*b*-poly (acrylic acid) (PS-*b*-PAA), and AuNPs tethered with polystyrene-*b*-poly (ethylene oxide) (PS-*b*-PEO) to function as imaging agents for PA and MR imaging of tumors (Fig. 5A) [182]. The observed high r_2 value (239.6 s^{-1} mM^{-1}) and strong absorption in the NIR range (redshift of absorption peak) of the JVs, attributed to the ordered and closer packing of MNPs and AuNPs in the vesicle membrane, make the hemispherically shaped structure more favorable than the spherical structure. Furthermore, the magnetic manipulation of the JVs enables local enrichment of Au materials and relatively slow heat dissipation to the surrounding water at the target site, resulting in excellent photothermal conversion efficiency. When JVs were intravenously injected into tumor-bearing mice and an applied magnetic field was used, a substantial increase in MR and PA signals at the tumor site was observed, demonstrating the JVs' dual-modality tumor imaging capability. This highlights the potential of the JVs for effective tumor imaging.

The integration of CPs with IONPs using amphiphilic polymers 1,2-distearoyl-*sn*-glycero-3-phosphoethanolamine-N [methoxy (poly (ethylene glycol))-2000] (mPEG2000-DSPE) has been developed as an optimized structure to enhance the multimodal imaging capabilities of magneto-optical nanosystems. This development has emerged as a crucial factor in the enhancement of the nanosystems' imaging ability. In addition to the hemispherical Janus structures mentioned previously, various configurations have been designed to achieve the desired enhancement. The research has identified the clever structural arrangement of components as an important aspect in this regard. Liu et al. developed a bimodal contrast agent, CP-IO, for photoacoustic-magnetic resonance imaging (PA-MRI) that exhibited a significantly amplified PA signal strength (Fig. 5B) [183]. The main UV–visible (UV-VIS) absorption peaks of the CP-IO nanocomposite possessed similar amplitudes and peak positions to those of bare CP and MIX nanoparticles, concentrating at 750 nm, signifying that the presence of IO nanoparticles did not affect the light absorption of CP (Fig. 5C). However, the CP-IO nanocomposites demonstrated a 45% stronger PA signal intensity than bare CP owing to the enhanced heat generation and dissipation pathway facilitated by the IO nanoparticles during the PA signal generation process, thereby facilitating improved PA image acquisition (Fig. 5D). Moreover, the T_2-weighted MR signal of the CP-IO nanocomposites gradually darkened as the concentration increased, with an average r_2 value of 98 mM^{-1} s^{-1} under the influence of IO nanoparticles, indicating the excellent T_2 MRI ability of CP-IO (Fig. 5E). The *in vivo* imaging results revealed that the injection of CP-IOs into the tail vein of mice led to their accumulation in the tumor area through EPR effects, consequently facilitating the generation of significant PA and MRI signals in the tumor area, enabling the acquisition of three-dimensional reconstructed PA and MRI images (Fig. 5F).

3.2. Multi-modal MRI/optical imaging

3.2.1. Multi-modal MRI/FLI/PAI

The integration of MRI, FLI, and PAI effectively overcomes the inherent limitations of each imaging modality. These include the relatively low sensitivity and time-consuming data acquisition process associated with MRI, the limited spatial resolution and inadequate depth penetration capabilities of FLI, as well as the restricted imaging area

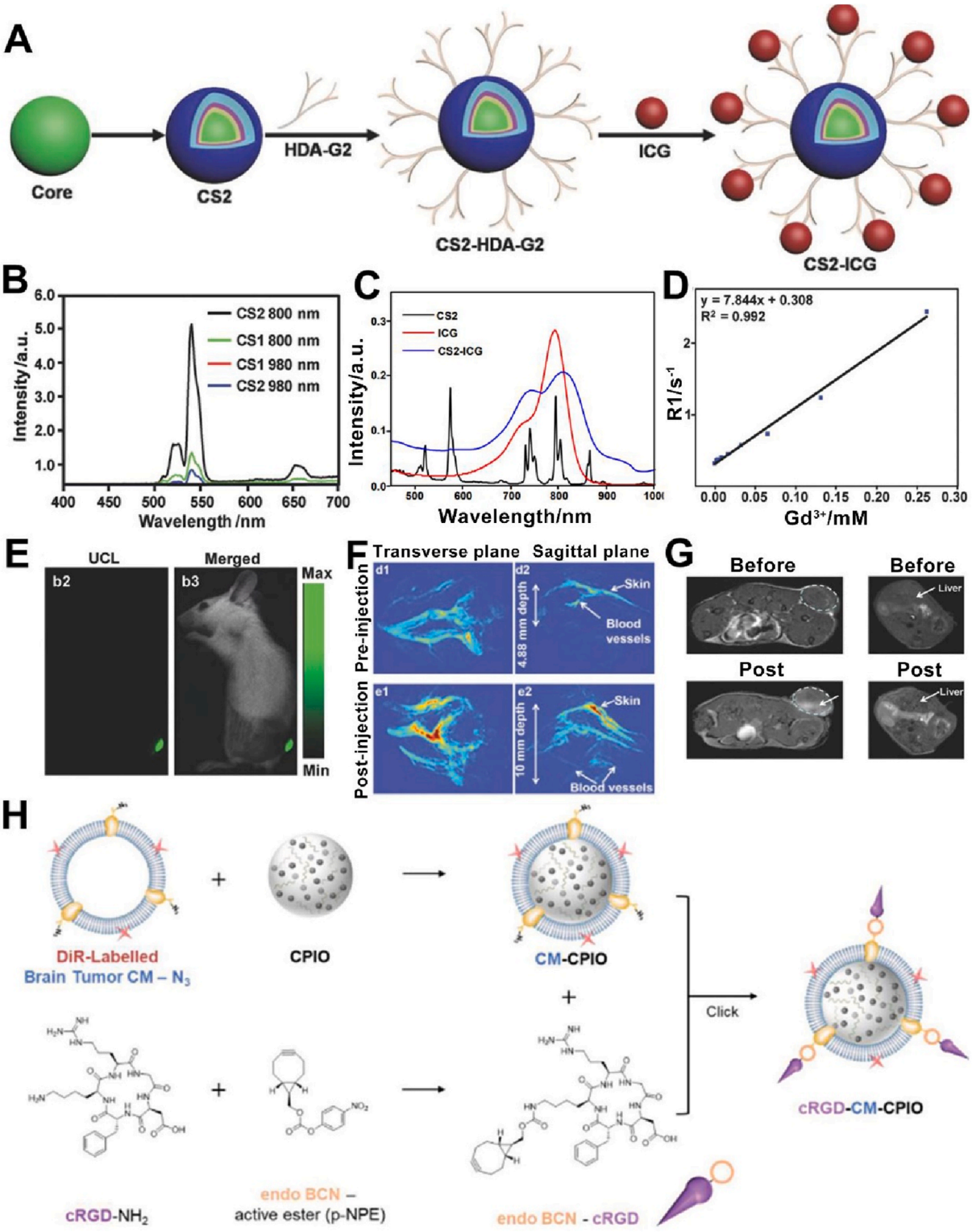

Fig. 6. (A) Schematic representation of the preparation of CS2-ICG. (B) UC spectra of CS irradiated with 980 or 800 nm laser. (C) UV-VIS absorption spectra of CS2, ICG and CS2-ICG. (D) The plot of relativity (R_1) of CS2-ICG. (E) In vivo UCL imaging of mice treated with UCNPs. (F–G) In vivo PAI (F) and MRI (G) of mice before and after injection. (H) Schematic representation of the preparation process of cRGD-CM-CPIO nanocomposites. [(A)–(G) reproduced with permission from Ref. [186], Copyright 2016, Wiley-VCH GmbH. (H) reproduced with permission from Ref. [188], Copyright 2020, Wiley-VCH GmbH].

provided by PAI. This amalgamation enables us to obtain more precise and comprehensive diagnostic information pertaining to various diseases [184,185]. Therefore, the utilization of magneto-optical nanosystems as a multifunctional probe for MRI/FLI/PAI holds great promise in clinical applications, particularly in precise tumor diagnosis.

Nie et al. prepared a CS_2-ICG nanocomposite material, which combined N-hydroxysuccinimide-labeled indocyanine green (ICG) (ICG-NHS) and multi-shell UCNPs consisting of NaYF4:Yb:Er@NaYF4:Yb@NaNdF4:Yb@NaYF4@NaGdF4 (CS_2) a dendritic molecule and 1-hexadecylamine (HAD-G2) [186]. Their findings realized three-mode

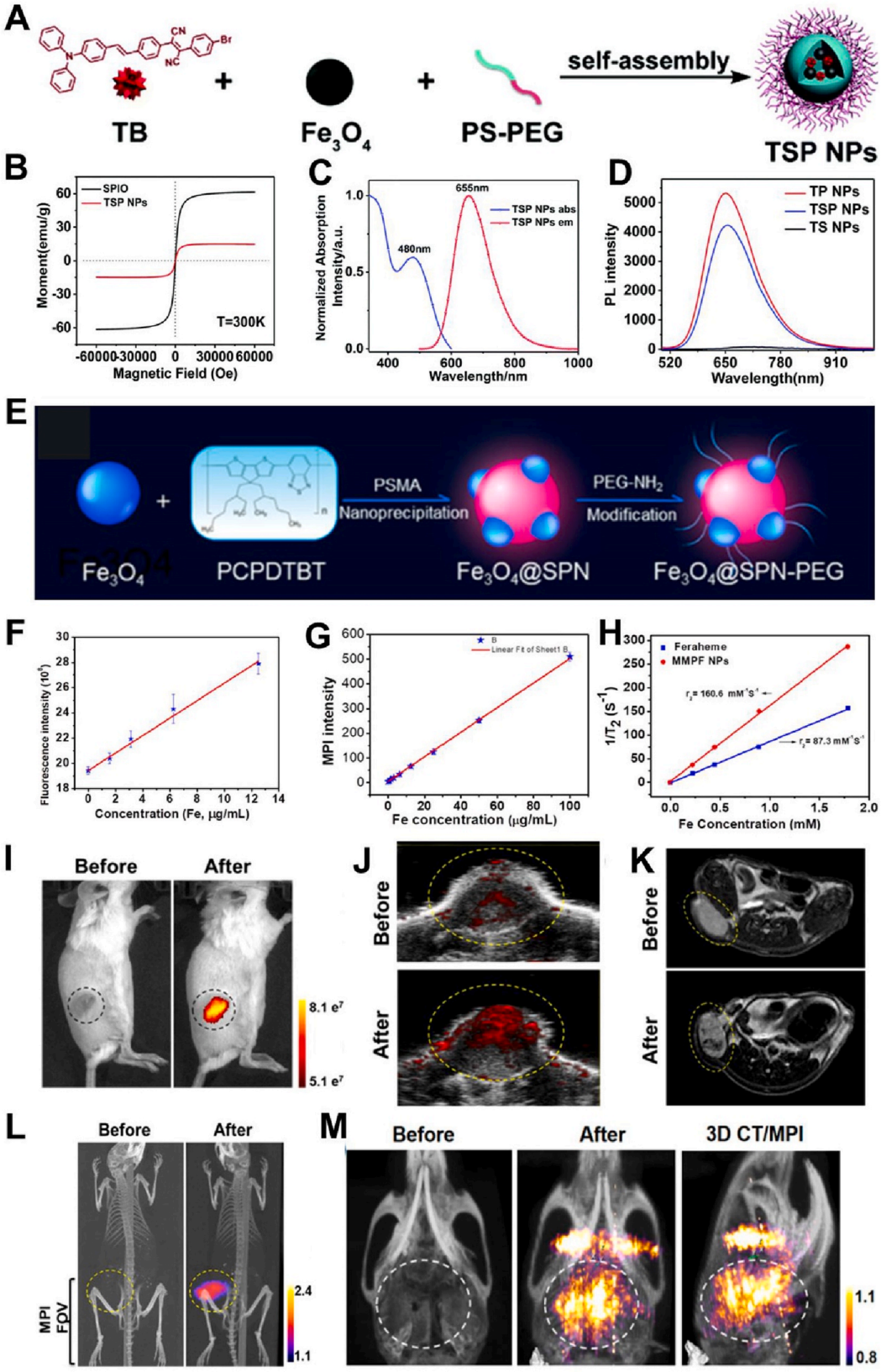

Fig. 7. (A) Schematic representation of the preparation of TSP NPs. (B) Magnetic measurements of TSP NPs and SPIO at 300 K. (C) UV-VIS absorption and emission spectra of TSP NPs. (D) PL spectra of the TP NPs, TSP NPs and TS. (E) Schematic representation of the preparation of MMPF NPs. (F) Correlation between fluorescence signal and Fe concentration in the low concentration range. (G) Correlation between MPI signal and Fe concentration from 0 to 100 μg/mL. (H) The plot of relaxation rate ($1/T_2$) of MMPF NPs. (I–L)) FLI (I), PAI (J), T_2-MRI (K), 3D-MPI/CT (L) of mice 4T1 subcutaneous tumor model 24 h before and after intravenous injection of MMPF NPs. (M) 3D MPI/CT images of orthotopic tumor mice models before and after intravenous injection of MMPF NPs. [(A)–(D) reproduced with permission from Ref. [193], Copyright 2019, Royal Society of Chemistry. (E)–(M) reproduced with permission from Ref. [194], Copyright 2019, American Chemical Society].

imaging capabilities for PAI, FLI, and MRI, paving the way for the clinical application of multi-modal imaging detection and collaborative therapy (Fig. 6A). The effective avoidance of back energy transfer from Er^{3+} to Nd^{3+} in CS_2, thanks to the doping of the activator (Er^{3+}) and sensitizer (Nd^{3+}) into different shells, resulted in a high UCL intensity. Furthermore, CS_2 exhibited an absolute QY of up to 0.75 ± 0.08% under 800 nm excitation light, demonstrating excellent UCL imaging potential (Fig. 6B) due to the photon transition of Er^{3+}. Additionally, the strong absorption capacity of Nd^{3+} in CS_2 under 800 nm laser irradiation, overlapping with that of ICG, resulted in substantial light absorption of CS_2-ICG in the NIR region, crucial for PAI (Fig. 6C). Moreover, the concentration-dependent increase in T_1-weighted MR signal strength of CS_2-ICG, with an r_1 relativity of 8.152 mM^{-1} s^{-1}, can be attributed to the dipolar interaction of the magnetic moments of the CS_2-ICG with protons in water (Fig. 6D). *In vivo* imaging results demonstrated significant enhancement of UCL, PA, and MR signals in mice after intravenous injection of CS_2-ICG, enabling highly sensitive and comprehensive detection of tumors through FLI, PAI, and MRI (Fig. 6E–G). These findings established a solid foundation for the further development and application of MR/FL/PA imaging probes in diagnosis and treatment.

Researchers have targeted magneto-optical nanosystems to overcome delivery barriers and improve the accumulation of nanocomposites at tumor sites due to various complications in the human body, such as the powerful blood-brain barrier (BBB) and the intricate tumor microenvironment [187]. Liu et al. developed a nanoscale multimodal MRI/FLI/PAI probe (cRGD-CM-CPIO), which consisted of a nanocomposite core composed of CP (PDPP3T) and ultrasmall IONPs, a brain tumor cell membrane (CM) doped with NIR lipophilic fluorophores (DiR), and integrin αVβ3 receptors target peptide cRGD [188]. This probe could quickly determine the specific location of brain tumors and delineate tumor edges for real-time imaging guided surgical treatment (Fig. 6H). The CM-CPIO exhibited a visible peak in its absorption spectrum at 750 nm in the presence of DiR dye and PDPP3T, showed excellent fluorescence and PA properties. It had the fluorescence characteristics of a DiR dye with a strong emission at 775 nm and a PA signal spectrum in the range of 700 nm–800 nm similar to the absorption spectrum class thanks to PDPP3T. Additionally, CM-CPIO effectively enhanced the T_2-weighted MRI signal because the magnetic properties of IONPs were little affected by the shell. The co-incubation experiment of brain tumor C6 cells with CPIO, CM-CPIO, and cRGD-CM-CPIO showed that CRGD-CM-CPIO had higher cell uptake and fluorescence intensity compared to the other two groups due to the effect of cRGD targeting integrin αvβ3 receptors on C6 cells in cRGD-CM-CPIO and the homotypic targeting of cell membrane coating. *In vivo* imaging results demonstrated that after injecting cRGD-CM-CPIO into the BALB/c nude mouse model of brain tumor, cRGD-CM-CPIO effectively penetrated the BBB *via* the targeting ability of cRGD ligand to BBB. This resulted in the enhanced fluorescence, PA and MR signals at the tumor site in the back brain of mice, enabling accurate imaging of brain tumors through FLI/PAI/MRI.

3.2.2. Multi-modal MPI/MRI/optical imaging

MPI is an imaging technique proposed in 2001 by Gleich et al., which directly derives its signal from the magnetic response of superparamagnetic nanoparticles under time-varying magnetic fields. This technique offers several advantages, including the ability to generate positive contrast without ionizing radiation, unlimited tissue penetration depth, low background noise, and high resolution [189,190]. By simultaneously enabling MPI and MRI, superparamagnetic MNPs can provide sensitive and accurate information about nanoparticle localization. Furthermore, when combined with other components, they can form magneto-optical nanosystems that offer additional optical imaging capabilities [191,192].

Tian et al. synthesized a fluorescence molecular imaging (FMI)/MPI/MRI multimodal probe, known as TB/SPIO@PS-PEG nanoparticles or TSP NPs. This probe was developed by encapsulating the fluorescent molecule 2-(4-bromophenyl)-3-(4-(4-(diphenylamino)styryl)phenyl) fumaronitrile (TB) and SPIO with polystyrene-PEG (PS-PEG). The TSP NPs were designed for tumor surveillance with high temporal-spatial resolution at an infinite depth (Fig. 7A) [193]. The incorporation of SPIO endowed TSP NP with superparamagnetic behavior similar to SPIO at room temperature, making it suitable as a T_2- MRI contrast agent with a transverse relaxation rate of 51.82 mM^{-1} s^{-1} (Fig. 7B). The UV-VIS absorption spectrum and PL spectrum of TSP NPs in aqueous solution revealed an absorption peak at 480 nm and an emission peak at 655 nm, with emissions extending beyond 950 nm in the NIR region (Fig. 7C). These characteristics indicated that TSP NPs were excellent for optical imaging as they exhibited less background interference and higher penetration depth due to the PL emission of the fluorescent molecule TB. Furthermore, the PS-PEG package prevented the fluorescence quenching of TSP NP, resulting in a 14.6% fluorescence QY and no significant reduction in fluorescence lifetime (Fig. 7D). Co-incubation of TSP NP-labeled HuH-7 cells showed a linear correlation between the fluorescence and MPI signals and the number of cells. When these labeled cells were implanted subcutaneously into nude mice, they were successfully monitored in real time for 24 days, demonstrating good long-term tracking ability. Additionally, in situ liver tumor monitoring using TPS NP showed deep penetration and high temporal-spatial resolution tumor information, highlighting the unique multimodal FMI/MRI/MPI approach.

Rao et al. prepared a Janus nanostructured multimodal cancer imaging nanosystem by nanoprecipitation (MMPF NP), comprising Fe_3O_4 nanoparticles, semiconductor polymer (PCPDTBT), modified amphiphilic polymer (PSMA), and PEG-NH_2 [194]. The generated nanosystem exhibited strong MPI, MRI, fluorescence, and PA signals for imaging tumor xenografts in living mice (Fig. 7E) [195]. The MPI contrast directly produced by the magnetic response of the tracer under a time-varying magnetic field was found to be proportional to the tracer mass. Scanning of diluted MMPF NP samples indicated a linear correlation between the MPI signal and the tracer concentration in the range of 0–100 μg/mL, with stability observed at low pH and high H_2O_2 concentration (Fig. 7F). Furthermore, the fluorescence signal emitted at 810 nm by MMPF NP, excited at 680 nm, exhibited good linearity in the low concentration range of Fe (0–12.5 μg/mL). The MMPF NP also demonstrated significant clinical potential for MRI, with a T_2 relaxation rate of 160.6 mM^{-1} s^{-1} at a 1.5T magnetic field (Fig. 7H). Injecting MMPF NP into mice showed an exceptionally long blood circulation time with a half-life of 49.16 h and higher tumor accumulation (18% ID/g). *In vivo* imaging results demonstrated a gradual increase in the intensity of FLI (Fig. 7I), PAI (Fig. 7J), MRI (Fig. 7K), and MPI (Fig. 7L and M) signals in the tumor area after intravenous injection of MMPF NP into the subcutaneous and in situ tumor models of mice, indicating good tumor contrast compared with normal tissues.

4. Image-guided cancer therapy

Image-guided therapy has emerged as a pivotal strategy in precision medicine, with the integration of multimodal imaging technology and magneto-optical nanosystems representing a significant breakthrough in tumor diagnostics [196,197]. This advancement enables precise tracking of pharmacokinetic processes, accurate guidance for various tumor therapies including photothermal therapy (PTT), chemotherapy, photodynamic therapy (PDT), and radiation therapy (RT), as well as real-time monitoring of treatment progress and outcomes. Consequently, this approach not only achieves precise tumor localization while minimizing damage to surrounding healthy tissues and organs but also provides visualization and monitoring capabilities for diseased tissue, delivery kinetics, and anticancer efficacy [198]. These attributes facilitate controlled adjustments to treatment strategies, making magneto-optical nanosystems highly promising for establishing multiple therapeutic systems suitable for precision medicine. Such advancements are instrumental in realizing effective targeted therapies while

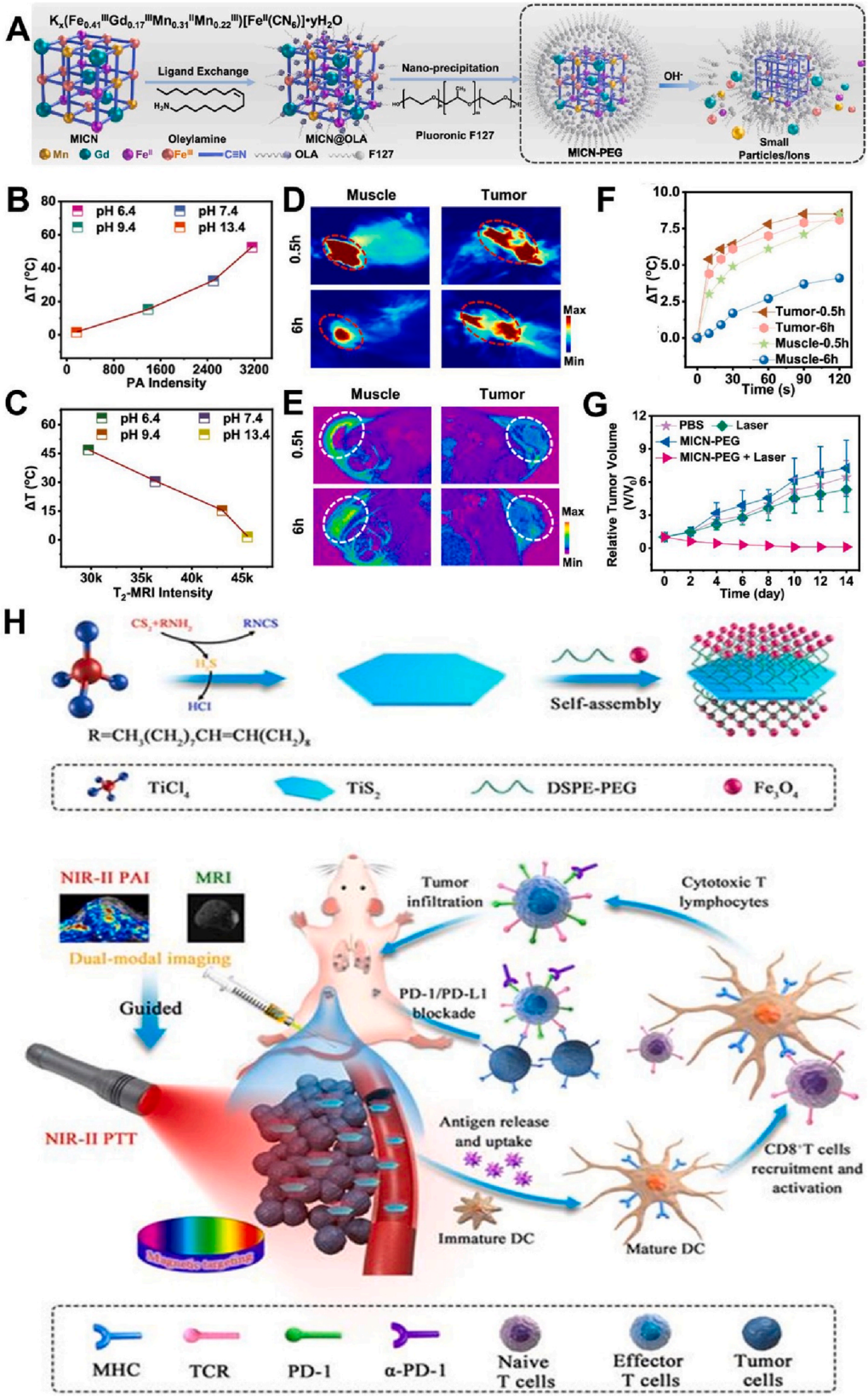

Fig. 8. (A) Schematic of MICN-PEG preparation and degradation in response to OH^-. (B–C) ΔT of PA signal (B) and T_2-MRI signal (C) under different pH conditions. (D–E) PA and T_2-MR images of muscle and tumor following MICN-PEG injection. (F) ΔT of mice muscle and tumor region after 808 nm laser irradiation. (G) Changes in tumor volume in mice treated with MICN-PEG + laser. (H) Schematic diagram of the process of PA/MR imaging of TSIO nanodrugs and imaging-guided PTT/immunotherapy. [(A)–(G) reproduced with permission from Ref. [201], Copyright 2022, American Chemical Societ. (H) reproduced with permission from Ref. [206], Copyright 2021, Ivyspring International].

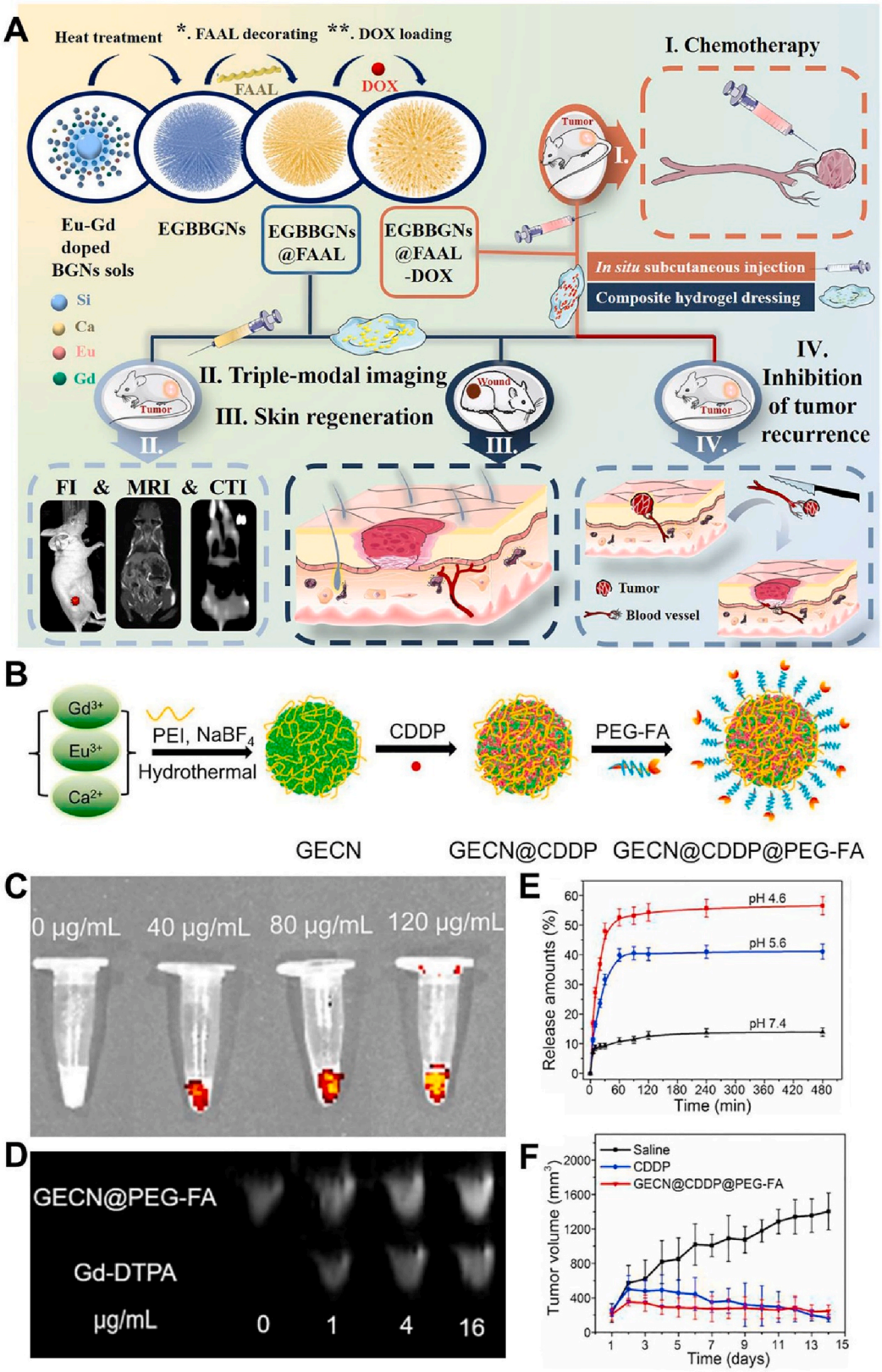

Fig. 9. (A) Schematic of the preparation and the process of performing multimodal imaging and chemotherapy of EGBBGN@FAAL. (B) Schematic of the preparation of GECN@CDDP@PEG-FA. (C) Fluorescence intensity of different concentrations of GECN@PEG-FA under 570 nm laser irradiation. (D) Comparison of T_1-weighted MRI of cells treated with GECN@PEG-FA and Gd-DTPA. (E) Graph of GECN@CDDP@PEG-FA release of CDDP over time at various pH. (F) Tumor volume change curves of mice after different treatments. [(A) reproduced with permission from Ref. [209], Copyright 2021, ScienceDirect. (B)–(F) reproduced with permission from Ref. [210], Copyright 2018, Elsevier].

enhancing drug efficacy and safety.

4.1. Image-guided PTT

PTT, a form of phototherapy for tumors, employs photothermal agents that absorb light in the NIR region to induce hyperthermia and selectively eradicate tumor cells. This noninvasive approach has gained significant attention due to its minimal damage to surrounding normal tissues [199,200]. Interestingly, certain magneto-optical nanosystems integrated with highly efficient photothermal conversion materials exhibit enhanced high optical and magnetic properties, offering promising prospects for effective multimodal imaging-guided PTT of tumors.

Song et al. successfully synthesized a biodegradable nanosystem, MICN-PEG, which possessed a framework structure consisting of Pluronic F127 (F127) encapsulated MICN formed by the coordination of magnetic ions (Fe^{III}, Fe^{II}, Gd^{III}, and Mn^{II}) and CN^- ligand [201]. This nanosystem exhibited pH-responsive structural collapse in normal tissues and demonstrated excellent performance in terms of PA signal generation, MRI, and PTT within the acidic tumor microenvironment (Fig. 8A). Due to the efficient charge transfer among Fe^{III}, Fe^{II}, Gd^{III}, and Mn^{II}, MICN-PEG exhibited strong NIR absorption at 720 nm, excellent PA signals (PA_{720}), and high photothermal effects within a narrow pH range. The presence of paramagnetic Fe, Gd, and Mn ions also contributed to the outstanding MRI performance of MICN-PEG by minimizing proton T_1 and T_2. Moreover, the PA signal and T_2-MRI signal showed positive or negative correlation with enhanced temperature (ΔT), indicating the potential of MIC-PEG for monitoring photothermal conversion efficiency. This was demonstrated in Fig. 8B and C. However, under alkaline conditions, OH^- triggered the degradation of MICN-PEG into smaller particles or ions leading to loss of charge transfer in MICN. Consequently, NIR absorption was significantly weakened with a sharp decrease in PA_{720} intensity and attenuated photothermal effect. Additionally, structural collapse of MICN-PEG results in reduced dipole-dipole interaction between magnetic ions and lower relaxation rates. These differences between acidic and alkaline environments suggested that MICN-PEG has the potential to enhance specificity in PA/MRI imaging while reducing toxic side effects. Following local injection of MICN-PEG into the muscle and tumor, the stability of PA_{720} and T_2-MRI signals in the tumor area ($PA_{6h}/PA_{0.5h} = 0.77$, $T_2\text{-}MRI_{0.5h}/T_2\text{-}MRI_{6h} = 0.94$) was significantly higher compared to that in the muscle area ($PA_{6h}/PA_{0.5h} = 0.27$, $T_2\text{-}MRI_{0.5h}/T_2\text{-}MRI_{6h} = 0.37$) (Fig. 8D and E). Furthermore, upon exposure to an 808 nm laser, a notable increase in local temperature was observed specifically within the tumor area in mice injected with MICN-PEG (Fig. 8F), resulting in inhibited tumor growth (Fig. 8G). These findings demonstrated that MICN-PEG exhibited excellent stability within the acidic tumor microenvironment while displaying favorable MRI, PAI, and photothermal ablation effects; thus, enabling differentiation between imaging signals and hyperthermia responses between tumors and normal tissues for enhanced specificity during tumor treatment.

The introduction of nanosystems with dual-modal FLI/MRI and PTT capabilities has expanded the options beyond just MRI/PAI-guided PTT. For example, Gao et al. developed self-assembled biocompatible nanoparticles (HSA-GGD-ICG NPs) composed of glycyrrhetinic-acid-modified gadolinium (III)-1,4,7,10-tetraazacyclododecane-1,4,7,10-tetraacetate (GGD), a MRI contrast agent; ICG, a fluorescence dye; and human serum albumin (HSA) [202]. These nanoparticles exhibited enhanced T_1-MRI and FLI capabilities as well as high photothermal conversion efficiency. HSA-GGD-ICG NPs displayed enhanced UV-VIS absorption and significantly increased fluorescence intensity compared with free ICG, as they effectively prevented the aggregation of ICG in aqueous solution and avoided its fluorescence quenching. Additionally, the larger volume and slower tumbling rate of HSA-GGD-ICG NPs resulted in a greater T_1 relativity compared to GGD molecules. This characteristic conferred excellent T_1-weighted MRI contrast ability under different magnetic fields. Moreover, when subjected to an 808 nm laser for 5 min, the HSA-GGD-ICG NPs aqueous solution exhibited a notable concentration-correlated temperature increase, with a photothermal conversion efficiency of 85.1%. This indicated the significant potential of HSA-GGD-ICG NPs in tumor PTT. Furthermore, co-incubation of HSA-GGD-ICG NPs with human hepatoma cells (HepG2) demonstrated strong fluorescence signal and effective mortality rate within the laser irradiation range, pointing to the effective tumor cell destruction by HSA-GGD-ICG NPs. *In vivo* imaging results revealed strong fluorescence and MRI signals at the tumor site in mice injected with HSA-GGD-ICG NPs, highlighting the *in vivo* stability, which facilitated their tumor accumulation through the EPR effect. Real-time monitoring and guidance of *in vivo* MRI and FLI showed that the tumors treated with HSA-GGD-ICG NPs and laser were severely damaged and gradually shrunk, accompanied by a significant temperature increase compared with other treatment groups. Furthermore, in addition to the bimodal imaging-guided PTT strategy, researchers have expanded the tri-modal MRI/FLI/PAI diagnostic integrated nanosystems to perform tumor diagnosis with finer images for guiding PTT. For example, Zhou et al. developed a nanoprobe encapsulated by poly (lactic-co-glycolic acid) perfluorocarbons and ICG to form a multifunctional therapeutic nanoprobe (AM-PP@ICG NPs), which could be used to determine tumor localization by MRI, obtain time-dependent tumor homing of NPs by FLI, and specific distribution of NPs within the tumor by PAI, and can also exhibit photothermal effects under NIR laser irradiation for effective PTT of tumors [203].

Numerous studies have demonstrated that PTT can effectively stimulate the release of tumor-associated antigens, thereby initiating a cascade of anti-tumor immune responses to complement the limitations of PTT as a standalone cancer treatment modality [204,205]. Consequently, the integration of PTT with immunotherapy has garnered significant attention for enhancing the therapeutic efficacy against cancer. Fu et al. prepared a multifunctional nanosystem (TSIO) for synergistic photothermal-immunotherapy of tumors under magnetic targeted dual-modal NIR-II PAI/MRI guidance (Fig. 8H) by anchoring IONPs onto the surface of TiS_2 nanosheets using a one-pot self-assembly technique [206]. The TSIO exhibited significantly enhanced NIR-II PA and T_2-weighted MR signal, allowing real-time monitoring of the treatment process, with MT effect resulting in a high accumulation of 17.9% at the tumor site under the external magnetic field. Analysis of the serum of mice in the TSIO with α-programmed cell death protein 1 (α-PD-1) treatment group revealed elevated levels of pro-inflammatory cytokines (including tumor necrosis factor α (TNF-α), interferon-γ (IFN-γ), interleukin-12 (IL-12)), indicating that PTT promoted the activation of immune responses. The results of mice tumor model experiments suggested that the combination of PTT and immunotherapy inhibited tumor growth, metastasis, and recurrence, thus opening new horizons for NIR–II–PA and MR image-guided PTT combination immunotherapy.

4.2. Image-guided chemotherapy

In recent decades, chemotherapy has been an important clinical treatment method for cancer patients due to its ability to kill tumor cells, inhibit their growth and proliferation, and promote differentiation. However, the non-specific distribution of drugs and serious side effects have limited its effectiveness [207,208]. The development of a magneto-optical nanosystem that combines chemotherapy drugs with diagnostic imaging probes has overcome these limitations by enabling multimodal imaging-guided chemotherapy. Lei et al. developed a multifunctional biodegradable silicon-based Eu-Gd-Si-Ca-based bioactive glass nanosystem (MBSGN), comprising of Eu–Gd doped branched bioactive glass nanoparticles (EGBBGNs), surface modifier FAAL molecules (alendronate (AL) grafted with folate (FA)), and the loaded chemotherapy drug doxorubicin hydrochloride (DOX). This platform enabled multimodal FL/MR/CT imaging of tumor tissue and provided guidance for chemotherapy (Fig. 9A) [209]. The modification of FAAL graft molecules resulted in improved dispersity of EGBBGNs in water

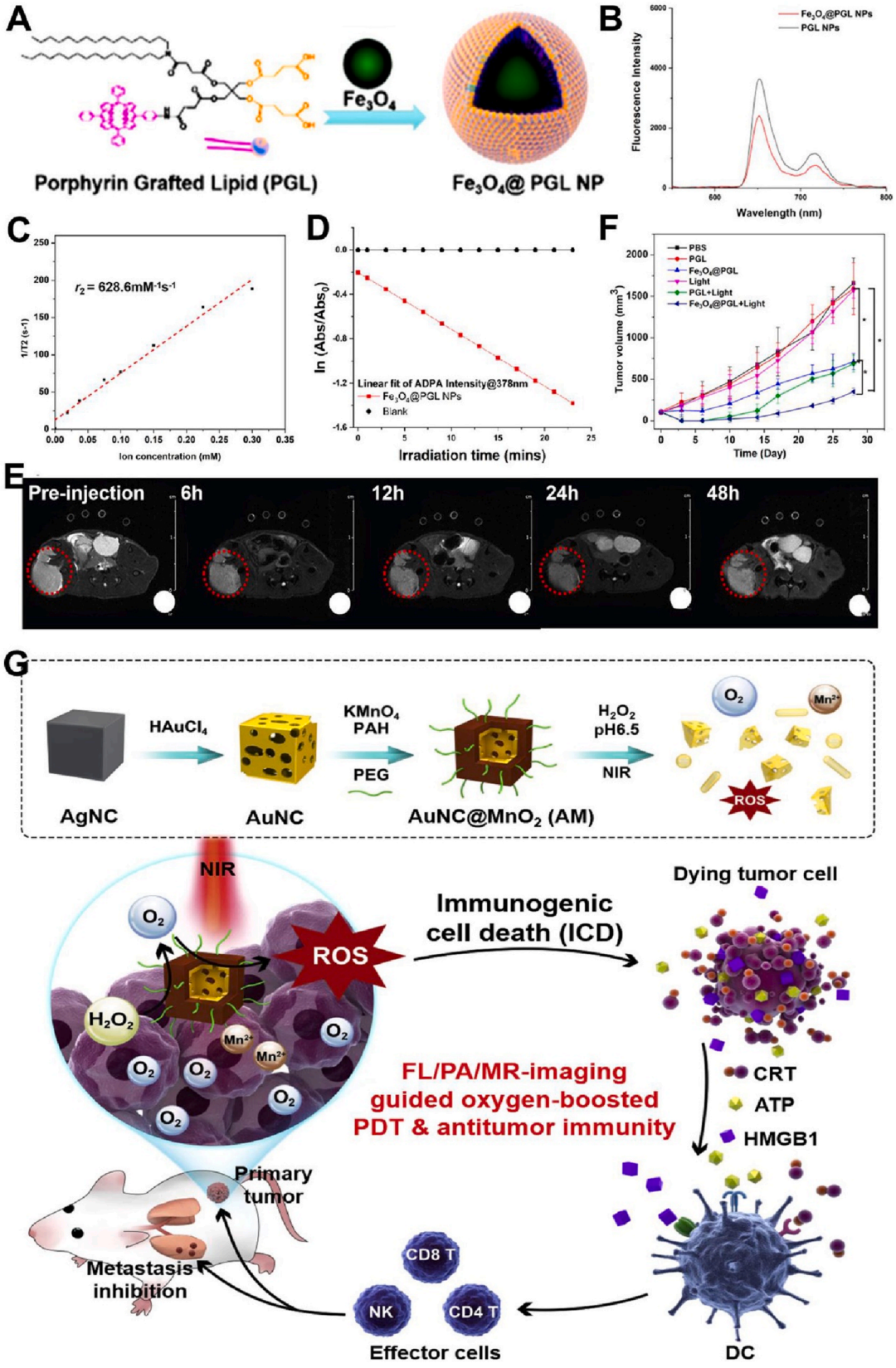

Fig. 10. (A) Schematic of the preparation of Fe_3O_4@PGL NPs. (B) Fluorescence emission spectra of Fe_3O_4@PGL NPs and Fe_3O_4 NPs under light excitation at 420 nm. (C) T_2 relaxation rates of Fe_3O_4@PGL NPs. (D) $^1O_2$ generation detected by the ADPA probe. (E) MR Images of tumors in mice after injection of Fe_3O_4@PGL NPs. (F) Tumor volume change curves of mice after different treatments. (G) Schematic of AM preparation and mechanism of action. [(A)–(E) reproduced with permission from Ref. [215], Copyright 2021, American Chemical Society. (G) reproduced with permission from Ref. [218], Copyright 2018, Elsevier].

and enhanced their ability to target tumor cells. Moreover, the protonation of their amino groups facilitated the loading of DOX drugs and led to a pH-responsive release with a cumulative drug release rate of 22.1% at pH 5.5 over 120 h. EGBBGNs@FAAL-DOX demonstrated promising magneto-optical performance and potential in FLI and MRI, attributable to the exceptional PL and magnetism of rare-earth-based nanoparticles. Notably, the electronic transition of the Eu^{3+} ion and the sensitization effect of Gd^{3+} on it contributed to the strong PL of EGBBGNs@FAAL, characterized by emission peaks at 589 and 613 nm under 393 nm light excitation. Additionally, EGBBGNs@FAAL exhibited excellent T_1-weighted imaging potential with a high r_1/r_2 value of 1.625 and CT imaging potential with 11.85 HU L g^{-1}. Importantly, *in vivo* imaging in mice following subcutaneous injection of EGBBGNs@FAAL showed significant tumor contrast for all three imaging modalities, thereby facilitating precise tumor localization. Consequently, compared to traditional Dox treatment, EGBBGNs@FAAL-DOX demonstrated superior anti-tumor therapeutic efficacy and biosafety due to pH-responsive release and guidance of imaging, leading to a significant reduction in tumor volume without a substantial impact on body weight.

In addition to employing surface modifiers for drug encapsulation, magneto-optical nanosystems can also be engineered with distinctive mesoporous structures to facilitate targeted drug delivery for cancer chemotherapy. Zou et al. developed a multifunctional nanosystem (GECN@CDDP@PEG-FA) for FL/MR imaging-guided cancer chemotherapy, incorporating polyethyleneimine (PEI)-driven self-assembled Eu-/Gd-doped CaF_2 nanoclusters (GECN), loaded cisplatin (CDDP), and PEG-coupled FA (Fig. 9B) [210]. The ordered mesoporous structure and high specific surface area of GECN resulted in a good CDDP loading capacity, achieving a drug capacity of 37.5 mg/g. CDDP responsively released in acidic environments, as the coordination between PEI's amino group and CDDP can be disrupted by the hydrogen proton. Furthermore, GECN@CDDP@PEG-FA doped with lanthanides exhibited excellent fluorescence properties and paramagnetic behavior, showing potential for FL and MR imaging. Cell incubation experiments demonstrated that the nanosystem, due to its appropriate size and positive charge, facilitated cellular internalization and enhanced fluorescence signals and MR image contrast (Fig. 9C and D). Upon tail vein injection into mice, GECN@CDDP@PEG-FA aggregated in tumor tissues through the EPR effect and recognition of overexpressed folate ligand on Hela cell membranes, consequently releasing CDDP in response to the acidic tumor microenvironment (Fig. 9E). This led to significant tumor growth inhibition in mice, as illustrated in Fig. 9F. Additionally, the stability of the body weight of GECN@CDDP@PEG-FA treated mice suggested effective alleviation of CDDP's side effects compared to free CDDP-treated mice.

4.3. Image-guided PDT

PDT is an alternative cancer phototherapy method that employs a photosensitizing agent to induce oxidative stress in cells during light irradiation, thereby generating ROS for the eradication of tumor cells [211,212]. In comparison with conventional treatment modalities such as chemotherapy, surgery, and PTT, PDT possesses distinct advantages including minimal drug resistance, non-invasiveness, and low phototoxicity [213,214]. Consequently, it has emerged as a promising candidate for tumor therapy. Recently, several magneto-optical nanosystems have been developed to enhance the tissue penetration depth and further augment the precision of PDT.

Dai et al. developed a multifunctional nanosystem by self-assembling porphyrin-grafted lipid (PGL) and DSPE-PEG on the hydrophobic surface of oleic acid-coated IONPs at a molar ratio of 9:1. This platform had the ability to guide cancer PDT through dual-modality FLI and MRI (Fig. 10A) [215]. Due to the presence of conjugated double bonds in porphyrins within PGL components, the UV-VIS absorption spectrum of Fe_3O_4@PGL NPs exhibits a distinct Soret band and a relatively weak Q-band within the wavelength range of 400–500 nm and 500–700 nm, respectively. Notably, the absorption peak closely resembles that observed for PGL alone, highlighting the minimal aggregation advantage displayed by Fe_3O_4@PGL NPs.Fe_3O_4@PGL NPs also demonstrated strong fluorescence at 650 nm, ensuring their applicability for FLI (Fig. 10B). Additionally, the Fe component of Fe_3O_4@PGL NPs imparted MRI feasibility with a lateral relaxation r_2 of 628.6 mM^{-1} s^{-1} (Fig. 10C). When subjected to singlet oxygen probe 9, 10-anthradipropionic acid disodium (ADPA), Fe_3O_4@PGL NPs rapidly generate $^1O_2$ under 650 nm laser irradiation with a QY of 0.27, indicating their potential for PDT (Fig. 10D). Co-incubation experiments with cells *in vitro* revealed that the fluorescence of Fe_3O_4@PGL NPs aligned with the staining area of lysosomes, suggesting their predominant presence in acidic lysosomes, conducive to the Fenton reaction of Fe_3O_4@PGL NPs to produce ROS. In the mouse model, intravenous injection of Fe_3O_4@PGL NPs resulted in both enhanced fluorescence signal and diminished T_2 signal intensity, providing insights into the accumulation of NPs at the tumor site, guiding imaging-based PDT, and ultimately leading to a reduction in tumor volume in mice (Fig. 10E and F).

Under exogenous light irradiation, PDT not only induces cell death by generating a substantial amount of ROS, but also triggers immunogenic cell death (ICD) and augments the anti-tumor immune response [216,217]. Recent studies have demonstrated that combining immunotherapy with PDT exhibits superior efficacy in tumor eradication. Cai et al. synthesized core-shell structured nanoparticles (AuNC@MnO_2, AM) using a template method, which consisted of hollow and porous gold nanocage as the core and a manganese dioxide shell [218]. This nanocomposite was designed for the purpose of PDT guided by PAI and MRI, as well as to induce an anti-tumor immune response in metastatic triple-negative breast cancer (mTNBC) (Fig. 10G). The MnO_2 shell of AM exhibited excellent in situ oxidation properties within the tumor microenvironment, enabling the degradation and release of O_2 in acidic conditions and in the presence of H_2O_2, thereby enhancing the PDT effect. In addition, the gold nanocages played a crucial role in generating ROS through hot electron-related photoreactions, energy, and electron transfer, as well as photocatalytic decomposition of H_2O_2 under NIR light irradiation. Consequently, AM was considered a promising photosensitizer with high NIR absorption. As indicated in Fig. 10K and L, the PA and MR signal intensities of AM were observed to increase with higher concentrations of Au and Mn^{2+} ions released from MnO_2 degradation, respectively, owing to the strong NIR absorption capability and high relaxation rate (r_1 = 8.050 mM^{-1} s^{-1}, pH 6.5 + H_2O_2). *In vitro* co-incubation experiments with murine 4T1 cells of mTNBC revealed that the AM + laser-treated cells elicited significantly higher levels of damage-associated molecular pattern, such as calreticulin, adenosine triphosphate, and high mobility group box-1 protein, and notably induced dendritic cells (DCs) activation compared to other groups, signifying that the AM-induced PDT enhances ICD progression. *In vivo* animal experiments showed a gradual increase in MR and PA signal intensity upon AM injection into 4T1 tumor xenograft mice, permitting real-time monitoring of AM, Mn^{2+}, and O_2 release. Furthermore, tumor growth and metastasis in mice were effectively inhibited and ultimately eliminated by the 15th day, with a substantial increase in mature DCs and immune cells, suggesting the potential of AM-induced PDT combined with anti-tumor immune response for effective tumor treatment.

4.4. Image-guided RT/PTT

RT, a crucial cancer treatment modality, utilizes high-energy ionizing radiation to eradicate tumors by targeting and eliminating cancer cells [219,220]. However, RT is hindered by challenges such as inaccurate tumor localization and resistance in clinical settings, which necessitates improvements in the efficacy of tumor therapy [221,222]. Fortunately, PTT emerges as a novel approach that not only induces localized hyperthermia for tumor cell ablation but also enhances the sensitivity of tumor cells to RT by promoting blood flow and oxygen partial pressure levels within the tumor tissue [223,224]. Moreover,

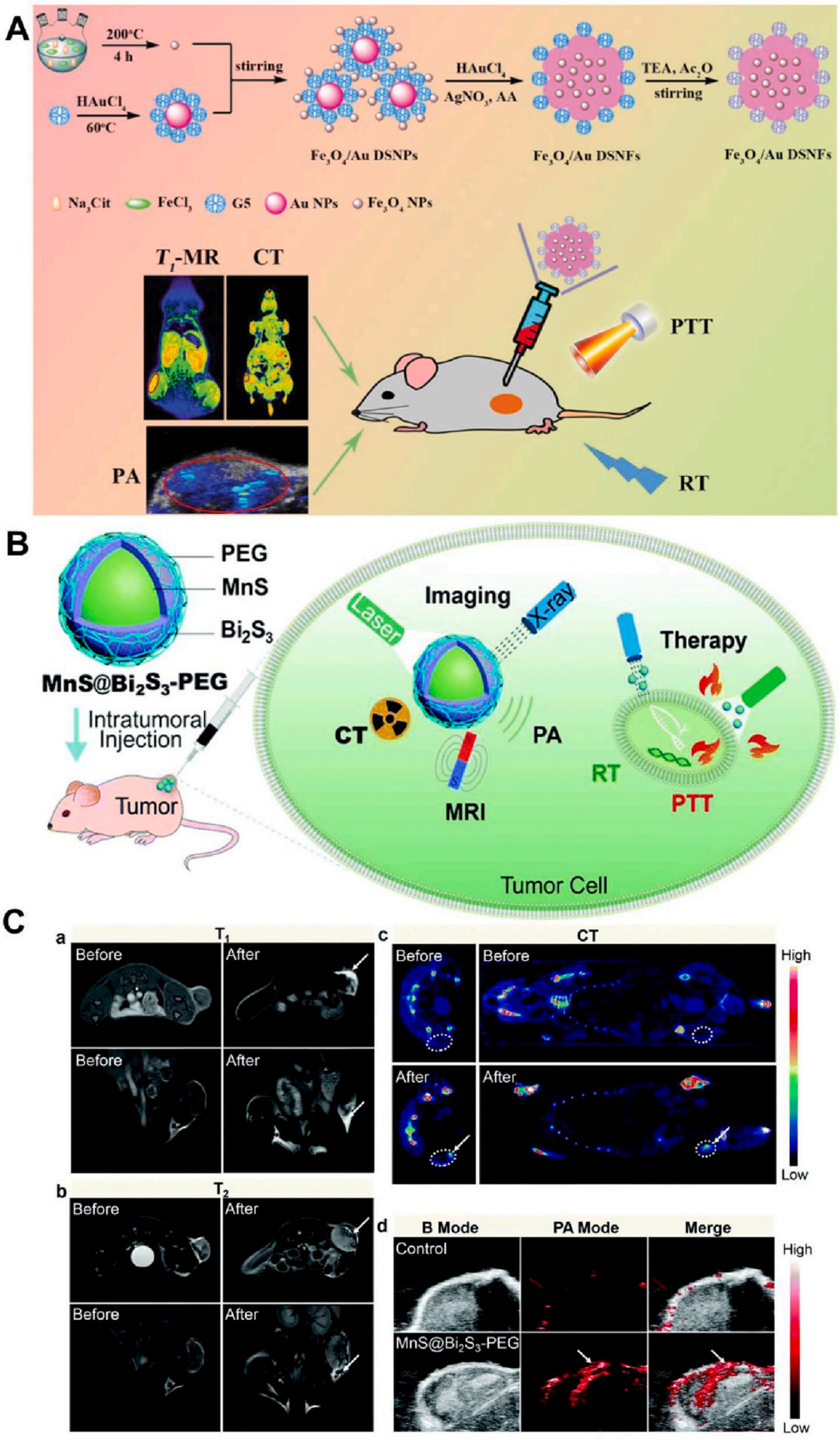

(caption on next page)

Fig. 11. (A) Schematic illustration of Fe_3O_4/Au DSNF synthesis and its application in multimodal imaging-guided radiotherapy/PTT. (B) Schematic representation of the structure of MnS@Bi_2S_3-PEG and its application to multimodal imaging and therapy. (C) The comparison of MRI (a and b), CT (c), and PAI (d) imaging in mice before and after injection of MnS@Bi_2S_3-PEG. [(A) reproduced with permission from Ref. [225], Copyright 2018, Wiley-VCH GmbH. (B)–(C) reproduced with permission from Ref. [228], Copyright 2017, Royal Society of Chemistry].

magneto-optical nanosystems enable multimodal imaging of tumors and facilitate combination therapies guided by this imaging technique, thereby augmenting the effectiveness of tumor treatment.

Shi et al. successfully synthesized a multifunctional composite therapeutic nanosystem, Fe_3O_4@Au NFs, through a seed-mediated approach. This platform consists of ultrasmall Fe_3O_4 nanoparticles (abbreviated as USIO NPs) and generation 5 (G5) poly (amidoamine) dendrimer-stabilized AuNFs, which enables tumor multimodal MR/CT/PA imaging and PTT/RT combination therapy (Fig. 11A) [225]. The aqueous solution of Fe_3O_4@Au DSNFs exhibited NIR peaks at 680–730 nm and a rapid temperature increase under laser irradiation, with a photothermal conversion efficiency of 82.7%, demonstrating its potential for PTT. The X-ray attenuation and radiosensitizing properties of AuNPs also render Fe_3O_4@Au DSNFs suitable for CT imaging and RT. In addition, the dispersed distribution of USIO NPs in Fe_3O_4@Au DSNFs enhanced their interaction with water protons, leading to the production of T_1-weighted MR imaging signals with a relativity of 3.2 mM^{-1} s^{-1}. *In vitro* cell experiments, treatment with Fe_3O_4@Au DSNFs at 2.0×10^{-3} M Au concentration in combination with 808 nm laser resulted in a significant reduction in the survival rate of 4T1 cells to 34.7%, indicating a photothermal ablation effect. Moreover, the *in vivo* mouse subcutaneous tumor model experiments demonstrated that Fe_3O_4@Au DSNFs act as tumor MR/CT/PA imaging contrast agents *via* the EPR effect, with maximum accumulation at 60 min after injection. Furthermore, tumors in mice subjected to laser irradiation followed by RT under the guidance of these imaging modalities were completely ablated after 4 days, indicating that Fe_3O_4@Au DSNFs had the potential for effective PTT combined with RT treatment under the guidance of trimodal tumor imaging.

In addition to gold, bismuth (Bi) is also a high atomic number element (Z = 83) with a significantly high X-ray attenuation coefficient of 5.74 cm^2 kg^{-1} [226,227]. Studies have demonstrated that when the concentration, size, and location of nanoparticles are identical, bismuth nanoparticles offer superior enhancement for X-ray source diagnosis compared to gold nanoparticles. Miao et al. conducted a study in which they prepared a nanocomposite material called MnS@Bi_2S_3-PEG NPs. This material has core-shell nanostructures formed through a cation exchange reaction, with a manganese sulfide (MnS) core, a bismuth sulfide (Bi_2S_3) shell, and surface modification with PEG. The MnS@Bi_2S_3-PEG NPs were developed for collaborative therapy using RT and PTT, guided by MR, CT, and PA imaging (Fig. 11B) [228]. These NPs possessed several imaging and therapeutic properties. Firstly, due to the presence of Mn^{2+} with five unpaired 3d electrons, the MnS@Bi_2S_3-PEG NPs exhibited excellent T_1-and T_2-weighted MR imaging capabilities, with respective relaxation rates (r_1 and r_2) of 5.33 mM^{-1} s^{-1} and 24.08 mM^{-1} s^{-1}. Additionally, the high-Z Bi element in the Bi_2S_3 shell provided a large X-ray attenuation coefficient, allowing the NPs to be utilized as radiosensitization and CT contrast agents, with Hounsfield unit (HU) values that increased linearly with Bi concentration. Furthermore, the Bi_2S_3 shell enabled the NPs to generate a PA signal proportional to their concentration under NIR laser irradiation at 892 nm. Additionally, these NPs converted light energy into heat under 808 nm NIR laser irradiation, indicating their potential as a contrast agent for PA imaging and a therapeutic agent for PTT. In cellular experiments using 4T1 cells, co-incubation with MnS@Bi_2S_3-PEG NPs followed by laser treatment and X-ray exposure led to a significant reduction in the number of viable tumor cells, demonstrating the NPs' effectiveness in inducing PTT and radiosensitization. *In vivo* animal experiments on BALB/c mice bearing 4T1 tumors, intratumoral injection of MnS@Bi_2S_3-PEG NPs resulted in a significant enhancement of MR, CT, and PA signals in the tumor area, facilitating more accurate tumor diagnosis (Fig. 11C). Moreover, mice treated with MnS@Bi_2S_3-PEG NPs and subjected to laser and X-ray irradiation exhibited more significant inhibition of tumor growth compared to other treatment groups, suggesting that MnS@Bi_2S_3-PEG NPs-induced PTT combined with RT hold promising therapeutic prospects under the guidance of trimodal tumor imaging.

4.5. Image-guided chemotherapy/PTT

Among the various combination therapies, chemotherapy/PTT has demonstrated synergistic efficacy with minimal adverse effects in preclinical studies. In recent years, several integrated magneto-optical nanosystems incorporating photothermal agents and chemotherapeutic drugs have been designed and developed, offering numerous advantages [229,230]. For instance, certain magneto-optical nanosystems not only possess magnetic and optical functionalities like MRI and PTT but also serve as effective nanocarriers for targeted delivery of chemotherapeutic drugs, thereby addressing issues related to drug stability, targeting efficiency during delivery, and potential side effects. Moreover, these magneto-optical nanosystems enable remote control over drug release kinetics from carriers, further enhancing therapeutic efficacy.

Zhang et al. developed multifunctional nanosystems (DOX@GNRs-MSNs-MA) by combining gold nanorods (GNRs-MSNs) coated with mesoporous silica shells (MSN), iron-based metal-organic frameworks (MOFs), and surface modifier hyaluronic acid (HA). This nanosystem allows the loading of chemotherapeutic agents, such as DOX, to achieve MR/CT/PA imaging-guided NIR-triggered combined chemotherapy-photothermal treatment (Fig. 12A) [231]. The GNRs-MSNs-MA platform exhibited MR imaging ability attributed to the iron-based MOF shell. The MR images darkened with increasing Fe concentration, demonstrating a T_2-weighted contrast ability with a ratio of r_2/r_1 of 9.8 (Fig. 12B). Additionally, the GNRs core provided X-ray attenuation properties for CT imaging and the platform showed light absorption properties in the NIR region enabling PA imaging. Furthermore, GNRs-MSNs-MA displayed a slightly red-shifted longitudinal surface plasmon resonance (SPR) band and a photothermal conversion efficiency of 27.5%, enabling rapid temperature rise under 808 nm laser irradiation and demonstrating stability (Fig. 12C). This photothermal effect facilitated the rapid release of loaded drugs and, due to the instability of MOF under acidic conditions, DOX was specifically released at the tumor site through acid and photothermal double response (Fig. 12D). The *in vitro* cell experiments demonstrated that DOX@GNRs-MSNs-MA exhibited greater cell uptake by 4T1 cells compared to other treatment groups, indicating its excellent cancer cell targeting ability attributed to the specific binding affinity of HA for CD44 receptor overexpressed on cancer cells. *In vivo* animal experiments revealed that the MR, CT, and PA signals in the tumor region of mice were gradually enhanced after intravenous injection of DOX@GNRs-MSNs-MA, confirming its tumor-targeting ability (Fig. 12E and F). This led to effective inhibition of tumor growth without significant changes in the mice's body weight after treatment, highlighting the therapeutic effect and excellent biocompatibility of DOX@GNRs-MSNs-MA in combined PTT and chemotherapy (Fig. 12G).

In addition to surface modifiers such as HA for targeted drug delivery, magneto-optical nanosystems have also been developed for precise drug delivery based on their inherent magnetic or optical properties, exhibiting promising potential in the field of oncology therapy. For example, Su et al. successfully constructed a yolk−shell multifunctional nanocapsule (GNR@IOs-DOX) comprised of GNRs, IO nanoshells,

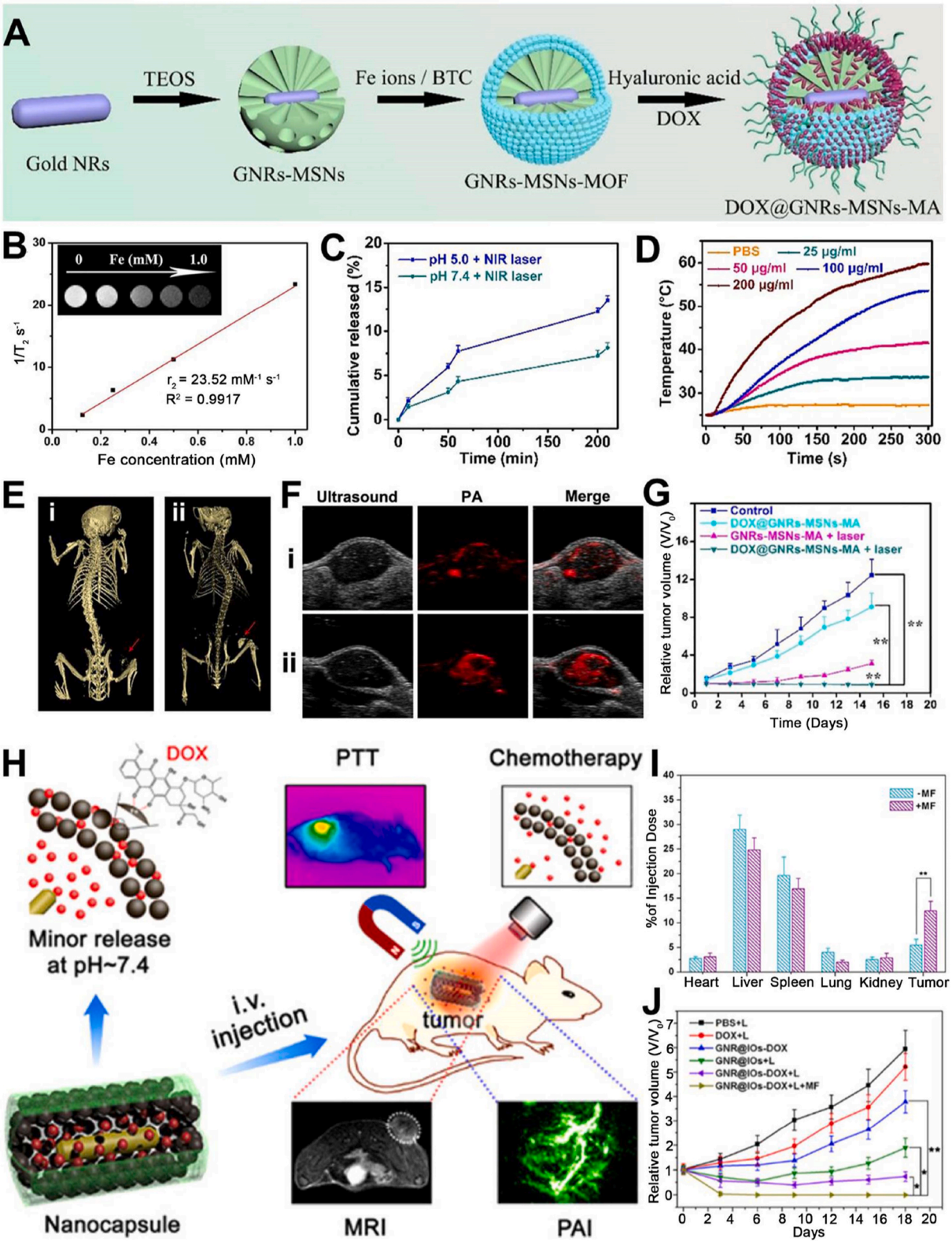

Fig. 12. (A) Schematic of the preparation process of DOX@GNRs-MSNs-MA. (B) The plot of the T_2 relaxation rate of GNRs-MSN-MA. (C) The amount of drug released of DOX@GNRs-MSNs-MA at different pH. (D) Temperature increase curve of GNRs-MSN-MA solution after irradiation with 808 nm laser. (E–F) CT (E) and PA (F) imaging in mice after intravenous administration of (i) GNRs-MSN-MOF and (ii) GNRs-MSN-MMA. (G) Curves of tumor volume changes in mice after different treatments. (H) Schematic of GNR@IOs-DOX drug release and mechanism of action for multimodal imaging as well as tumor therapy. (I) Distribution of Au in various organs of mice 24 h after IV injection of GNR@IOs-DOX. (J) Curves of tumor volumes in mice after different treatments. [(A)–(G) reproduced with permission from Ref. [231], Copyright 2021, Elsevier. (H)–(J) reproduced with permission from Ref. [232], Copyright 2016, American Chemical Society].

Table 2
Summary of magneto-optical nanosystems and their applications.

Magneto-optical nanosystem	Diagnostic application	Treatment application	Ref
MICN-PEG	MRI/PAI	PTT	[201]
TSIO	MRI/PAI	PTT/ Immunotherapy	[206]
MBSGN	MRI/FLI/CT	Chemotherapy	[209]
GECN@CDDP@PEG-FA	MRI/FLI	Chemotherapy	[210]
Fe_3O_4@PGL NPs	MRI/FLI	PDT	[215]
AuNC@MnO_2	MRI/PAI	PDT	[218]
Fe_3O_4@Au NFs	MRI/PAI/CT	PTT/RT	[225]
MnS@Bi_2S_3-PEG NPs	MRI/PAI/CT	PTT/RT	[228]
DOX@GNRs-MSNs-MA	MRI/PAI/CT	Chemotherapy/PTT	[231]
GNR@IOs-DOX	MRI/PAI	Chemotherapy/PTT	[232]

chemotherapy drug DOX, and dopamine-modified HA (DA-HA) by using SPION instead of a silica matrix [232]. This nanocapsule achieved tumor clearance by combining PTT and chemotherapy, guided by MRI/PAI dual-modal imaging (Fig. 12H). The GNR@IOs-DOX exhibited strong magnetic response characteristics with a high saturation magnetization of 42.5 $emug^{-1}$ owing to the mesoporous structure of the IO nanoshell, making it a potential candidate for *in vivo* magnetic tumor targeting. Additionally, the nanocapsules demonstrated excellent plasma properties attributed to the remaining gold surface chemistry and monodispersity resulting from silica protection during the thermal decomposition process. This was mainly reflected by the LSPR peak at the NIR absorption properties at 807 nm and the significant increase in temperature under 808 nm laser irradiation for PTT. Due to these properties, GNR@IOs-DOX was employed as r_2 for T_2-weighted MRI contrast agent with 177 mM^{-1} s^{-1}, PA imaging contrast agent, and photothermal agent. Furthermore, the plasma and hollow/permeable nanostructures of GNR@IOs-DOX conferred it with drug delivery and pH/NIR laser dual-response release capabilities, allowing for acid-responsive release of DOX through the formation or disruption of metal-ligand ligand bonds by external pH changes, and further stimulated release of NIR laser by local heating to enhance free diffusion. *In vitro* cellular experiments revealed greater cellular uptake through receptor-mediated endocytosis in cells co-incubated with GNR@IOs-DOX compared to other treatment groups, as evident from confocal laser scanning microscopy and flow cytometry. In vivo mouse model experiments, the MR and PA signals within the tumor region of 4T1 tumor-bearing mice were gradually enhanced after intravenous injection of GNR@IOs-DOX and the application of an external magnetic field, indicating the targeted enrichment of the nanodrug at the tumor site through the EPR effect and external magnetic guidance (Fig. 12I). Furthermore, after enrichment in the tumor region, GNR@IOs-DOX was subjected to 808 nm laser irradiation and led to a significant suppression of tumor volume in mice, resulting in a 100% survival rate within 30 days, thus affirming the excellent therapeutic efficacy and biocompatibility of GNR@IOs-DOX-induced PTT and chemotherapy combination therapy (Fig. 12J). This study underscored the potential of magneto-optical nanosystems for magnetically guided drug targeting and NIR laser-controlled tumor PTT, thus presenting a promising avenue for future research in this field.

5. Conclusions and prospects

The magneto-optical nanosystem, a composite nanomaterial that integrates magnetism and optical properties, has found extensive applications in various fields such as physics, chemistry, and biomedicine due to its dual functionality. In recent years, research on magneto-optical nanosystems as a platform for disease diagnosis and treatment has focused on two main aspects: firstly, the development of additional types of magneto-optical nanosystems to explore their functions and values further; secondly, the optimization of existing magneto-optical nanosystems through chemical modification or functionalization to advance their applications. This review presents different types of magneto-optical nanosystems including iron oxide-based and other magnetic material-based systems while highlighting their recent advancements in multimodal imaging and image-guided tumor treatments (Table 2).

With the advancement of contemporary medical technology, the integration of multimodal imaging and diagnosis with treatment has transitioned from conceptualization to practical applications. However, despite extensive research on magneto-optical nanosystems in these domains, their translation into clinical practice remains elusive due to significant challenges such as inadequate biocompatibility and suboptimal tissue biodistribution. Furthermore, most magneto-optical nanosystems for diagnostic and therapeutic purposes are still at the proof-of-concept stage necessitating further exploration. Considering these issues and challenges, we propose potential directions for the development of multifunctional magneto-optical nanosystems for multimodal imaging and therapy.

Firstly, ensuring biosafety is crucial for the clinical translation of magneto-optical nanosystems. Although numerous studies have confirmed the favorable biosafety profile of magneto-optical nanosystems, these experiments are currently limited to short-term evaluations in mouse models. It is important to note that certain materials may exhibit a prolonged latency period for toxicity and could potentially lead to the development of various diseases over time. Therefore, comprehensive assessment of the long-term toxicity of magneto-optical nanosystems through preclinical testing is urgently needed to mitigate potential adverse effects. Furthermore, future research should prioritize the design of intelligent and safer magneto-optical nanosystems. The rational integration of magnetic and photoresponsive release mechanisms or multimodal therapy can overcome limitations associated with single-stimulus responsiveness and synergistically contribute towards effective tumor therapy.

Secondly, the precise dosage of each constituent in the nanosystem plays a pivotal role in determining the overall properties of the magneto-optical nanosystem. For instance, optical materials used for FL imaging are typically employed at lower concentrations compared to magnetic materials utilized for MR imaging. Hence, it is imperative to meticulously consider and evaluate the dose ratio of each component during nanosystem preparation to ensure optimal performance.

In the realm of future research, a promising avenue could involve employing magneto-optical nanosystems to establish real-time efficacy assessment systems for clinical applications. Real-time efficacy assessment, as opposed to conventional tumor efficacy assessment methods, holds the potential to aid doctors in promptly adjusting treatment plans and mitigating the side effects of ineffective therapies. Presently, clinical efficacy assessment methods typically necessitate weeks or months post-treatment for determining tumor therapy effectiveness or entail invasive procedures. Henceforth, establishing non-invasive early efficacy assessment is imperative for enhancing tumor treatment effectiveness and improving patients' quality of life. The optical properties inherent in magneto-optical nanoplatforms enable highly sensitive, non-invasive imaging with rapid feedback capabilities, thereby exhibiting significant potential for real-time efficacy assessment in clinical settings.

In conclusion, magneto-optical nanosystems exhibit promising potential applications in biomedicine. Despite encountering several obstacles that need to be overcome, we firmly believe that through collaborative efforts from researchers across diverse fields encompassing magnetism, optics, material chemistry, and biomedicine; This integrated platform will ultimately realize its full potential for clinical utilization.

CRediT authorship contribution statement

Mengzhen Wang: Writing – original draft, Formal analysis, Data curation. **Yin Wang:** Visualization, Resources, Methodology, Investigation. **Qinrui Fu:** Writing – review & editing, Project administration,

Funding acquisition, Conceptualization.

Declaration of competing interest

The authors declare that they have no known competing financial interests or personal relationships that could have appeared to influence the work reported in this paper.

Data availability

No data was used for the research described in the article.

Acknowledgments

This work was supported by the Taishan Scholar Youth Expert Program in Shandong Province (Grant Number: tsqnz20230608), Scientific Research of Distinguished Professor from Qingdao University, China (Grant Number: DC2200000953), grants from the Natural Science Foundation of Shandong Province (Grant Number: ZR2023QB045), and grants from Natural Science Foundation of Qingdao Municipality, Shandong Province, China (Grant Number: 23-2-1-30-zyyd-jch).

References

[1] M. Mabrouk, D.B. Das, Z.A. Salem, H.H. Beherei, Nanomaterials for biomedical applications: production, characterisations, recent trends and difficulties, Molecules 26 (2021), https://doi.org/10.3390/molecules26041077.
[2] L. Sun, H. Liu, Y. Ye, Y. Lei, R. Islam, S. Tan, R. Tong, Y.-B. Miao, L. Cai, Smart nanoparticles for cancer therapy, Signal Transduct. Targeted Ther. 8 (2023) 418, https://doi.org/10.1038/s41392-023-01642-x.
[3] S. Karki, M.B. Gohain, D. Yadav, P.G. Ingole, Nanocomposite and bio-nanocomposite polymeric materials/membranes development in energy and medical sector: a review, Int. J. Biol. Macromol. 193 (2021) 2121–2139, https://doi.org/10.1016/j.ijbiomac.2021.11.044.
[4] K.H. Shen, C.H. Lu, C.Y. Kuo, B.Y. Li, Y.C. Yeh, Smart near infrared-responsive nanocomposite hydrogels for therapeutics and diagnostics, J. Mater. Chem. B 9 (2021) 7100–7116, https://doi.org/10.1039/d1tb00980j.
[5] S. Behrens, I. Appel, Magnetic nanocomposites, Curr. Opin. Biotechnol. 39 (2016) 89–96, https://doi.org/10.1016/j.copbio.2016.02.005.
[6] Z. Huang, J. Gong, Z. Nie, Symmetry-breaking synthesis of multicomponent nanoparticles, Acc. Chem. Res. 52 (2019) 1125–1133, https://doi.org/10.1021/acs.accounts.9b00038.
[7] Y. Ding, X. Hong, Y. Liu, H. Zhang, Recent advances in magnetic upconversion nanocomposites for bioapplications, Curr. Pharmaceut. Des. 25 (2019) 2007–2015, https://doi.org/10.2174/1381612825666190708202403.
[8] H. Peng, G. Ren, N. Hampp, A. Wu, F. Yang, The development of rare-earth combined Fe-based magnetic nanocomposites for use in biological theranostics, Nanoscale 15 (2023) 10513–10528, https://doi.org/10.1039/d3nr01373a.
[9] C. Xu, Y. Liu, J. Li, P. Ning, Z. Shi, W. Zhang, Z. Li, R. Zhou, Y. Tong, Y. Li, C. Lv, Y. Shen, Q. Cheng, B. He, Y. Cheng, Photomagnetically powered spiky nanomachines with thermal control of viscosity for enhanced cancer mechanotherapy, Adv. Mater. 35 (2023) 2204996, https://doi.org/10.1002/adma.202204996.
[10] K.-L. Chen, Y.-S. Lin, J.-M. Chen, C.-H. Wu, C.-C. Jeng, L.-M. Wang, A sensitive platform for in vitro immunoassay based on biofunctionalized magnetic nanoparticles and magneto-optical Faraday effect, Sensor. Actuator. B Chem. 258 (2018) 947–951, https://doi.org/10.1016/j.snb.2017.11.144.
[11] L. Xu, Y. Luo, Q. Du, W. Zhang, L. Hu, N. Fang, J. Wang, J. Liu, J. Zhou, Y. Zhong, Y. Liu, H. Ran, D. Guo, J. Xu, Magnetic response combined with bioactive ion therapy: a RONS-scavenging theranostic nanoplatform for thrombolysis and renal ischemia–reperfusion injury, ACS Nano 17 (2023) 5695–5712, https://doi.org/10.1021/acsnano.2c12091.
[12] A. Tomitaka, H. Arami, A. Ahmadivand, N. Pala, A.J. McGoron, Y. Takemura, M. Febo, M. Nair, Magneto-plasmonic nanostars for image-guided and NIR-triggered drug delivery, Sci. Rep. 10 (2020) 10115, https://doi.org/10.1038/s41598-020-66706-2.
[13] X. Zhang, Z. Zeng, H. Liu, L. Xu, X. Sun, J. Xu, G. Song, Recent development of a magneto-optical nanoplatform for multimodality imaging of pancreatic ductal adenocarcinoma, Nanoscale 14 (2022) 3306–3323, https://doi.org/10.1039/d1nr08394e.
[14] Y. Feng, D. Ding, W. Sun, Y. Qiu, L. Luo, T. Shi, S. Meng, X. Chen, H. Chen, Magnetic manganese oxide sweetgum-ball nanospheres with large mesopores regulate tumor microenvironments for enhanced tumor nanotheranostics, ACS Appl. Mater. Interfaces 11 (2019) 37461–37470, https://doi.org/10.1021/acsami.9b11843.
[15] S. Yang, Y. Song, H. Dong, Y. Hu, J. Jiang, S. Chang, J. Shao, D. Yang, Stimuli-actuated turn-on theranostic nanoplatforms for imaging-guided antibacterial treatment, Small 19 (2023) 2304127, https://doi.org/10.1002/smll.202304127.
[16] X. Huang, Z.-h. Zhang, J. Chen, Z. Mao, H. Zhu, Y. Liu, Z. Zhu, H. Chen, One dimensional magneto-optical nanocomplex from silver nanoclusters and magnetite nanorods containing ordered mesocages for sensitive detection of PD-L1, Biosens. Bioelectron. 189 (2021) 113385, https://doi.org/10.1016/j.bios.2021.113385.
[17] Q. Zhang, S. Liu, H. Zheng, H. Wang, G. Luo, X. Zhang, C. Du, J. Chen, Magnetic photoactive Fe3O4@Sb2S3 nanospheres assisted homogeneous photoelectrochemical–electrochemical biosensing platform integrating with MOFs-derived bifunctional NPC@Thi nanopolyhedra-mediated dual "signal-on" strategy for protein tyrosine kinase activity, Chem. Eng. J. 476 (2023) 146592, https://doi.org/10.1016/j.cej.2023.146592.
[18] B.R. Smith, S.S. Gambhir, Nanomaterials for in vivo imaging, Chem. Rev. 117 (2017) 901–986, https://doi.org/10.1021/acs.chemrev.6b00073.
[19] N. Lee, D. Yoo, D. Ling, M.H. Cho, T. Hyeon, J. Cheon, Iron oxide based nanoparticles for multimodal imaging and magnetoresponsive therapy, Chem. Rev. 115 (2015) 10637–10689, https://doi.org/10.1021/acs.chemrev.5b00112.
[20] D. Gao, Z. Sheng, Y. Liu, D. Hu, J. Zhang, X. Zhang, H. Zheng, Z. Yuan, Protein-modified CuS nanotriangles: a potential multimodal nanoplatform for in vivo tumor photoacoustic/magnetic resonance dual-modal imaging, Adv. Healthcare Mater. 6 (2017) 1601094, https://doi.org/10.1002/adhm.201601094.
[21] M. Zhang, W. Wang, Y. Cui, X. Chu, B. Sun, N. Zhou, J. Shen, Magnetofluorescent Fe3O4/carbon quantum dots coated single-walled carbon nanotubes as dual-modal targeted imaging and chemo/photodynamic/photothermal triple-modal therapeutic agents, Chem. Eng. J. 338 (2018) 526–538, https://doi.org/10.1016/j.cej.2018.01.081.
[22] X. Dai, Z. Fan, Y. Lu, P.C. Ray, Multifunctional nanoplatforms for targeted multidrug-resistant-bacteria theranostic applications, ACS Appl. Mater. Interfaces 5 (2013) 11348–11354, https://doi.org/10.1021/am403567k.
[23] T.H. Shin, Y. Choi, S. Kim, J. Cheon, Recent advances in magnetic nanoparticle-based multi-modal imaging, Chem. Soc. Rev. 44 (2015) 4501–4516, https://doi.org/10.1039/c4cs00345d.
[24] Z. Ma, J. Mohapatra, K. Wei, J.P. Liu, S. Sun, Magnetic nanoparticles: synthesis, anisotropy, and applications, Chem. Rev. 123 (2023) 3904–3943, https://doi.org/10.1021/acs.chemrev.1c00860.
[25] S. Wang, Z. Wang, Y. Hou, Self-assembled magnetic nanomaterials: versatile theranostics nanoplatforms for cancer, Aggregate 2 (2021), https://doi.org/10.1002/agt2.18.
[26] R. Qiao, C. Fu, H. Forgham, I. Javed, X. Huang, J. Zhu, A.K. Whittaker, T.P. Davis, Magnetic iron oxide nanoparticles for brain imaging and drug delivery, Adv. Drug Deliv. Rev. 197 (2023) 114822, https://doi.org/10.1016/j.addr.2023.114822.
[27] C. Qi, W. Wang, P. Wang, H. Cheng, X. Wang, B. Gong, A. Xie, Y. Shen, Facile synthesis of Fe3O4@Au/PPy-DOX nanoplatform with enhanced glutathione depletion and controllable drug delivery for enhanced cancer therapeutic efficacy, Molecules 27 (2022) 4003.
[28] R. Lv, X. Jiang, F. Yang, Y. Wang, M. Feng, J. Liu, J. Tian, Degradable magnetic-response photoacoustic/up-conversion luminescence imaging-guided photodynamic/photothermal antitumor therapy, Biomater. Sci. 7 (2019) 4558–4567, https://doi.org/10.1039/C9BM00853E.
[29] L. Lei, B. Nan, F. Yang, L. Xu, G. Guan, J. Xu, R. Yue, Y. Wang, S. Huan, X. Yin, X.-B. Zhang, G. Song, Zinc–carnosine metallodrug network as dual metabolism inhibitor overcoming metabolic reprogramming for efficient cancer therapy, Nano Lett. 23 (2023) 2659–2668, https://doi.org/10.1021/acs.nanolett.2c05029.
[30] Y. Hu, S. Mignani, J.P. Majoral, M. Shen, X. Shi, Construction of iron oxide nanoparticle-based hybrid platforms for tumor imaging and therapy, Chem. Soc. Rev. 47 (2018) 1874–1900, https://doi.org/10.1039/c7cs00657h.
[31] L. Zhang, Y. Liu, H. Huang, H. Xie, B. Zhang, W. Xia, B. Guo, Multifunctional nanotheranostics for near infrared optical imaging-guided treatment of brain tumors, Adv. Drug Deliv. Rev. 190 (2022) 114536, https://doi.org/10.1016/j.addr.2022.114536.
[32] X.-l. Tang, F. Jing, B.-l. Lin, S. Cui, R.-t. Yu, X.-d. Shen, T.-w. Wang, pH-responsive magnetic mesoporous silica-based nanoplatform for synergistic photodynamic therapy/chemotherapy, ACS Appl. Mater. Interfaces 10 (2018) 15001–15011, https://doi.org/10.1021/acsami.7b19797.
[33] A. Tomitaka, H. Arami, A. Ahmadivand, N. Pala, A.J. McGoron, Y. Takemura, M. Febo, M. Nair, Magneto-plasmonic nanostars for image-guided and NIR-triggered drug delivery, Sci. Rep. 10 (2020) 10115, https://doi.org/10.1038/s41598-020-66706-2.
[34] A.I. Martínez-Banderas, A. Aires, M. Quintanilla, J.A. Holguín-Lerma, C. Lozano-Pedraza, F.J. Teran, J.A. Moreno, J.E. Perez, B.S. Ooi, T. Ravasi, J.S. Merzaban, A. L. Cortajarena, J. Kosel, Iron-based core–shell nanowires for combinatorial drug delivery and photothermal and magnetic therapy, ACS Appl. Mater. Interfaces 11 (2019) 43976–43988, https://doi.org/10.1021/acsami.9b17512.
[35] T.-H. Yan, M. Yuan, N. Nguyen, J. Chen, X. Feng, T. Fan, M.C. Harnett, Z. Xiao, Y. Li, J.-P. Pellois, H.-C. Zhou, Y. Wang, Surface-modified gold-coated superparamagnetic iron oxide nanoparticles promoting light-controlled drug release, Adv. Compos. Hybrid Mater. 6 (2023) 226, https://doi.org/10.1007/s42114-023-00811-4.
[36] Q. Zhang, W. Wang, M. Zhang, F. Wu, T. Zheng, B. Sheng, Y. Liu, J. Shen, N. Zhou, Y. Sun, A theranostic nanocomposite with integrated black phosphorus nanosheet, Fe3O4@MnO2-doped upconversion nanoparticles and chlorin for simultaneous multimodal imaging, highly efficient photodynamic and photothermal therapy, Chem. Eng. J. 391 (2020), https://doi.org/10.1016/j.cej.2019.123525.
[37] M. Zhang, B. Sheng, J. Ashley, T. Zheng, W. Wang, Q. Zhang, J. Zhang, N. Zhou, J. Shen, Y. Sun, Manganese ion chelated FeOCl@PB@PDA@BPQDs

nanocomposites as a tumor microenvironment-mediated nanoplatform for enhanced tumor imaging and therapy, Sensor. Actuator. B Chem. 307 (2020), https://doi.org/10.1016/j.snb.2019.127491.
[38] S.-L. Li, P. Jiang, F.-L. Jiang, Y. Liu, Recent advances in nanomaterial-based nanoplatforms for chemodynamic cancer therapy, Adv. Funct. Mater. 31 (2021) 2100243, https://doi.org/10.1002/adfm.202100243.
[39] M. Ravichandran, G. Oza, S. Velumani, J.T. Ramirez, F. Garcia-Sierra, N. B. Andrade, A. Vera, L. Leija, M.A. Garza-Navarro, Plasmonic/magnetic multifunctional nanoplatform for cancer theranostics, Sci. Rep. 6 (2016) 34874, https://doi.org/10.1038/srep34874.
[40] F. Yang, A. Skripka, M.S. Tabatabaei, S.H. Hong, F. Ren, Y. Huang, J.K. Oh, S. Martel, X. Liu, F. Vetrone, D. Ma, Magnetic photoluminescent nanoplatform built from large-pore mesoporous silica, Chem. Mater. 31 (2019) 3201–3210, https://doi.org/10.1021/acs.chemmater.9b00028.
[41] X. Ma, Y. Wang, X.-L. Liu, H. Ma, G. Li, Y. Li, F. Gao, M. Peng, H.M. Fan, X.-J. Liang, Fe3O4–Pd Janus nanoparticles with amplified dual-mode hyperthermia and enhanced ROS generation for breast cancer treatment, Nanoscale Horiz 4 (2019) 1450–1459, https://doi.org/10.1039/C9NH00233B.
[42] H. Wang, Q. Mu, R. Revia, K. Wang, B. Tian, G. Lin, W. Lee, Y.-K. Hong, M. Zhang, Iron oxide-carbon core-shell nanoparticles for dual-modal imaging-guided photothermal therapy, J. Contr. Release 289 (2018) 70–78, https://doi.org/10.1016/j.jconrel.2018.09.022.
[43] M. Colombo, S. Carregal-Romero, M.F. Casula, L. Gutierrez, M.P. Morales, I. B. Bohm, J.T. Heverhagen, D. Prosperi, W.J. Parak, Biological applications of magnetic nanoparticles, Chem. Soc. Rev. 41 (2012) 4306–4334, https://doi.org/10.1039/c2cs15337h.
[44] T. Wang, Y. Zhou, C. Lei, J. Luo, S. Xie, H. Pu, Magnetic impedance biosensor: a review, Biosens. Bioelectron. 90 (2017) 418–435, https://doi.org/10.1016/j.bios.2016.10.031.
[45] L.-S. Lin, X. Yang, Z. Zhou, Z. Yang, O. Jacobson, Y. Liu, A. Yang, G. Niu, J. Song, H.-H. Yang, X. Chen, Yolk–shell nanostructure: an ideal architecture to achieve harmonious integration of magnetic–plasmonic hybrid theranostic platform, Adv. Mater. 29 (2017) 1606681, https://doi.org/10.1002/adma.201606681.
[46] N.T. Dung, N.V. Long, L.T.T. Tam, P.H. Nam, L.D. Tung, N.X. Phuc, L.T. Lu, N. T. Kim Thanh, High magnetisation, monodisperse and water-dispersible CoFe@Pt core/shell nanoparticles, Nanoscale 9 (2017) 8952–8961, https://doi.org/10.1039/C6NR09325F.
[47] I. Srivastava, R. Xue, J. Jones, H. Rhee, K. Flatt, V. Gruev, S. Nie, Biomimetic surface-enhanced Raman scattering nanoparticles with improved dispersibility, signal brightness, and tumor targeting functions, ACS Nano 16 (2022) 8051–8063, https://doi.org/10.1021/acsnano.2c01062.
[48] T. Li, T. Zhang, The application of nanomaterials in angiogenesis, Curr. Stem Cell Res. Ther. 16 (2021) 74–82, https://doi.org/10.2174/1574888x15666200211102203.
[49] T. Liu, Y. Lu, R. Zhan, W. Qian, G. Luo, Nanomaterials and nanomaterials-based drug delivery to promote cutaneous wound healing, Adv. Drug Deliv. Rev. 193 (2023) 114670, https://doi.org/10.1016/j.addr.2022.114670.
[50] Y. Zhao, Z. Zhang, Z. Pan, Y. Liu, Advanced bioactive nanomaterials for biomedical applications, Explorations 1 (2021) 20210089, https://doi.org/10.1002/EXP.20210089.
[51] W. Liu, L. Chen, M. Chen, W. Wang, X. Li, H. Yang, S. Yang, Z. Zhou, Self-amplified apoptosis targeting nanoplatform for synergistic magnetic–thermal/chemo therapy in vivo, Adv. Healthcare Mater. 9 (2020) 2000202, https://doi.org/10.1002/adhm.202000202.
[52] J. Wang, Z. Fang, C. Zhao, Z. Sun, S. Gao, B. Zhang, D. Qiu, M. Yang, F. Sheng, S. Gao, Y. Hou, Intelligent size-switchable iron carbide-based nanocapsules with cascade delivery capacity for hyperthermia-enhanced deep tumor ferroptosis, Adv. Mater. 35 (2023) 2307006, https://doi.org/10.1002/adma.202307006.
[53] M. Naghdi, M. Ghovvati, N. Rabiee, S. Ahmadi, N. Abbariki, S. Sojdeh, A. Ojaghi, M. Bagherzadeh, O. Akhavan, E. Sharifi, M. Rabiee, M.R. Saeb, K. Bolouri, T. J. Webster, E.N. Zare, A. Zarrabi, Magnetic nanocomposites for biomedical applications, Adv. Colloid Interface Sci. 308 (2022) 102771, https://doi.org/10.1016/j.cis.2022.102771.
[54] R. Guo, H. Peng, Y. Tian, S. Shen, W. Yang, Mitochondria-targeting magnetic composite nanoparticles for enhanced phototherapy of cancer, Small 12 (2016) 4541–4552, https://doi.org/10.1002/smll.201601094.
[55] F.-C. Lin, Y. Xie, T. Deng, J.I. Zink, Magnetism, ultrasound, and light-stimulated mesoporous silica nanocarriers for theranostics and beyond, J. Am. Chem. Soc. 143 (2021) 6025–6036, https://doi.org/10.1021/jacs.0c10098.
[56] Y. Wu, X. Song, W. Xu, K.-y. Sun, Z. Wang, Z. Lv, Y. Wang, Y. Wang, W. Zhong, J. Wei, H.-L. Cai, X. Wu, NIR-activated multimodal photothermal/chemodynamic/magnetic resonance imaging nanoplatform for anticancer therapy by Fe(II) ions doped MXenes (Fe-Ti3C2), Small 17 (2021) 2101705, https://doi.org/10.1002/smll.202101705.
[57] Y. Luo, Z. Chen, S. Wen, Q. Han, L. Fu, L. Yan, D. Jin, J.-C.G. Bünzli, G. Bao, Magnetic regulation of the luminescence of hybrid lanthanide-doped nanoparticles, Coord. Chem. Rev. 469 (2022), https://doi.org/10.1016/j.ccr.2022.214653.
[58] E.A. Kwizera, E. Chaffin, Y. Wang, X. Huang, Synthesis and properties of magnetic-optical core-shell nanoparticles, RSC Adv. 7 (2017) 17137–17153, https://doi.org/10.1039/C7RA01224A.
[59] M. Estrader, K. Soulantica, B. Chaudret, Organometallic synthesis of magnetic metal nanoparticles, Angew. Chem. Int. Ed. 61 (2022) e202207301, https://doi.org/10.1002/anie.202207301.
[60] S. Mourdikoudis, A. Kostopoulou, A.P. LaGrow, Magnetic nanoparticle composites: synergistic effects and applications, Adv. Sci. 8 (2021) 2004951, https://doi.org/10.1002/advs.202004951.
[61] J. Yang, J. Feng, S. Yang, Y. Xu, Z. Shen, Exceedingly small magnetic iron oxide nanoparticles for T1-weighted magnetic resonance imaging and imaging-guided therapy of tumors, Small 49 (2023) 2302856, https://doi.org/10.1002/smll.202302856.
[62] S. Wang, Y. Hou, New types of magnetic nanoparticles for stimuli-responsive theranostic nanoplatforms, Adv. Sci. 10 (2023) 2305459, https://doi.org/10.1002/advs.202305459.
[63] M.J. Ko, S. Min, H. Hong, W. Yoo, J. Joo, Y.S. Zhang, H. Kang, D.-H. Kim, Magnetic nanoparticles for ferroptosis cancer therapy with diagnostic imaging, Bioact. Mater. 32 (2024) 66–97, https://doi.org/10.1016/j.bioactmat.2023.09.015.
[64] X. Li, W. Li, M. Wang, Z. Liao, Magnetic nanoparticles for cancer theranostics: advances and prospects, J. Contr. Release 335 (2021) 437–448, https://doi.org/10.1016/j.jconrel.2021.05.042.
[65] A. Tripathy, M.J. Nine, F.S. Silva, Biosensing platform on ferrite magnetic nanoparticles: synthesis, functionalization, mechanism and applications, Adv. Colloid Interface Sci. 290 (2021) 102380, https://doi.org/10.1016/j.cis.2021.102380.
[66] D. Lisjak, A. Mertelj, Anisotropic magnetic nanoparticles: a review of their properties, syntheses and potential applications, Prog. Mater. Sci. 95 (2018) 286–328, https://doi.org/10.1016/j.pmatsci.2018.03.003.
[67] S. Tong, H. Zhu, G. Bao, Magnetic iron oxide nanoparticles for disease detection and therapy, Mater. Today 31 (2019) 86–99, https://doi.org/10.1016/j.mattod.2019.06.003.
[68] T. Lam, P. Pouliot, P.K. Avti, F. Lesage, A.K. Kakkar, Superparamagnetic iron oxide based nanoprobes for imaging and theranostics, Adv. Colloid Interface Sci. 199–200 (2013) 95–113, https://doi.org/10.1016/j.cis.2013.06.007.
[69] Y. Yang, Y. Liu, L. Song, X. Cui, J. Zhou, G. Jin, A.R. Boccaccini, S. Virtanen, Iron oxide nanoparticle-based nanocomposites in biomedical application, Trends Biotechnol. 41 (2023) 1471–1487, https://doi.org/10.1016/j.tibtech.2023.06.001.
[70] N.A. Frey, S. Peng, K. Cheng, S. Sun, Magnetic nanoparticles: synthesis, functionalization, and applications in bioimaging and magnetic energy storage, Chem. Soc. Rev. 38 (2009) 2532–2542, https://doi.org/10.1039/b815548h.
[71] S. Thangudu, C.-C. Yu, C.-L. Lee, M.-C. Liao, C.-H. Su, Magnetic, biocompatible FeCO3 nanoparticles for T2-weighted magnetic resonance imaging of in vivo lung tumors, J. Nanobiotechnol. 20 (2022) 157, https://doi.org/10.1186/s12951-022-01355-3.
[72] X. Lu, H. Zhou, Z. Liang, J. Feng, Y. Lu, L. Huang, X. Qiu, Y. Xu, Z. Shen, Biodegradable and biocompatible exceedingly small magnetic iron oxide nanoparticles for T1-weighted magnetic resonance imaging of tumors, J. Nanobiotechnol. 20 (2022) 350, https://doi.org/10.1186/s12951-022-01562-y.
[73] G. Ren, X. Zhou, R. Long, M. Xie, R.K. Kankala, S. Wang, Y.S. Zhang, Y. Liu, Biomedical applications of magnetosomes: state of the art and perspectives, Bioact. Mater. 28 (2023) 27–49, https://doi.org/10.1016/j.bioactmat.2023.04.025.
[74] P. Xue, R. Yang, L. Sun, Q. Li, L. Zhang, Z. Xu, Y. Kang, Indocyanine green-conjugated magnetic prussian blue nanoparticles for synchronous photothermal/photodynamic tumor therapy, Nano-Micro Lett. 10 (2018) 74, https://doi.org/10.1007/s40820-018-0227-z.
[75] Z.-j. Zhang, Z.-t. Liu, Y.-p. Huang, W. Nguyen, Y.-x. Wang, L. Cheng, H. Zhou, Y. Wen, L. Xiong, W. Chen, Magnetic resonance and fluorescence imaging superparamagnetic nanoparticles induce apoptosis and ferroptosis through photodynamic therapy to treat colorectal cancer, Mater. Today Phys. 36 (2023) 101150, https://doi.org/10.1016/j.mtphys.2023.101150.
[76] T. Kang, F. Li, S. Baik, W. Shao, D. Ling, T. Hyeon, Surface design of magnetic nanoparticles for stimuli-responsive cancer imaging and therapy, Biomaterials 136 (2017) 98–114, https://doi.org/10.1016/j.biomaterials.2017.05.013.
[77] J. Mosayebi, M. Kiyasatfar, S. Laurent, Synthesis, functionalization, and design of magnetic nanoparticles for theranostic applications, Adv. Healthcare Mater. 6 (2017) 1700306, https://doi.org/10.1002/adhm.201700306.
[78] R.S. Das, D. Maiti, S. Kar, T. Bera, A. Mukherjee, P.C. Saha, A. Mondal, S. Guha, Design of water–soluble rotaxane-capped superparamagnetic, ultrasmall Fe3O4 nanoparticles for targeted NIR fluorescence imaging in combination with magnetic resonance imaging, J. Am. Chem. Soc. 145 (2023) 20451–20461, https://doi.org/10.1021/jacs.3c06232.
[79] P. Martinkova, M. Brtnicky, J. Kynicky, M. Pohanka, Iron oxide nanoparticles: innovative tool in cancer diagnosis and therapy, Adv. Healthcare Mater. 7 (2018) 1700932, https://doi.org/10.1002/adhm.201700932.
[80] Z. Zhao, M. Li, J. Zeng, L. Huo, K. Liu, R. Wei, K. Ni, J. Gao, Recent advances in engineering iron oxide nanoparticles for effective magnetic resonance imaging, Bioact. Mater. 12 (2022) 214–245, https://doi.org/10.1016/j.bioactmat.2021.10.014.
[81] M. Jung, H. Kim, J.W. Hwang, Y. Choi, M. Kang, C. Kim, J. Hong, N.K. Lee, S. Moon, J.W. Chang, S.-j. Choi, S.-y. Oh, H. Jang, D.L. Na, B.-S. Kim, Iron oxide nanoparticle-incorporated mesenchymal stem cells for alzheimer's disease treatment, Nano Lett. 23 (2023) 476–490, https://doi.org/10.1021/acs.nanolett.2c03682.
[82] C. Marques, M.J. Hajipour, C. Marets, A. Oudot, R. Safavi-sohi, M. Guillemin, G. Borchard, O. Jordan, L. Saviot, L. Maurizi, Identification of the proteins determining the blood circulation time of nanoparticles, ACS Nano 17 (2023) 12458–12470, https://doi.org/10.1021/acsnano.3c02041.

[83] N. Daviu, Y. Portilla, M. Gómez de Cedrón, A. Ramírez de Molina, D.F. Barber, DMSA-coated IONPs trigger oxidative stress, mitochondrial metabolic reprograming and changes in mitochondrial disposition, hindering cell cycle progression of cancer cells, Biomaterials 304 (2024) 122409, https://doi.org/10.1016/j.biomaterials.2023.122409.
[84] X. Liu, M. Wang, Y. Jiang, X. Zhang, C. Shi, F. Zeng, Y. Qin, J. Ye, J. Hu, Z. Zhou, Magnetic resonance imaging nanoprobe quantifies nitric oxide for evaluating M1/M2 macrophage polarization and prognosis of cancer treatments, ACS Nano 17 (2023), https://doi.org/10.1021/acsnano.3c05627.
[85] S. Liu, B. Yu, S. Wang, Y. Shen, H. Cong, Preparation, surface functionalization and application of Fe3O4 magnetic nanoparticles, Adv. Colloid Interface Sci. 281 (2020) 102165, https://doi.org/10.1016/j.cis.2020.102165.
[86] R.A. Revia, M. Zhang, Magnetite nanoparticles for cancer diagnosis, treatment, and treatment monitoring: recent advances, Mater, Today Off. 19 (2016) 157–168, https://doi.org/10.1016/j.mattod.2015.08.022.
[87] M. Tadic, S. Kralj, L. Kopanja, Synthesis, particle shape characterization, magnetic properties and surface modification of superparamagnetic iron oxide nanochains, Mater. Char. 148 (2019) 123–133, https://doi.org/10.1016/j.matchar.2018.12.014.
[88] Z. Zhou, L. Yang, J. Gao, X. Chen, Structure-relaxivity relationships of magnetic nanoparticles for magnetic resonance imaging, Adv. Mater. 31 (2019) e1804567, https://doi.org/10.1002/adma.201804567.
[89] S.M. Dadfar, K. Roemhild, N.I. Drude, S. von Stillfried, R. Knuchel, F. Kiessling, T. Lammers, Iron oxide nanoparticles: diagnostic, therapeutic and theranostic applications, Adv. Drug Deliv. Rev. 138 (2019) 302–325, https://doi.org/10.1016/j.addr.2019.01.005.
[90] Y. Xiao, J. Du, Superparamagnetic nanoparticles for biomedical applications, J. Mater. Chem. B 8 (2020) 354–367, https://doi.org/10.1039/C9TB01955C.
[91] N. Lamichhane, S. Sharma, Parul, A.K. Verma, I. Roy, T. Sen, Iron oxide-based magneto-optical nanocomposites for in vivo biomedical applications, Biomedicines 9 (2021), https://doi.org/10.3390/biomedicines9030288.
[92] U. Resch-Genger, M. Grabolle, S. Cavaliere-Jaricot, R. Nitschke, T. Nann, Quantum dots versus organic dyes as fluorescent labels, Nat. Methods 5 (2008) 763–775, https://doi.org/10.1038/nmeth.1248.
[93] H. Moon, C. Lee, W. Lee, J. Kim, H. Chae, Stability of quantum dots, quantum dot films, and quantum dot light-emitting diodes for display applications, Adv. Mater. 31 (2019) 1804294, https://doi.org/10.1002/adma.201804294.
[94] J. Ning, B. Zhang, L. Siqin, G. Liu, Q. Wu, S. Xue, T. Shao, F. Zhang, W. Zhang, X. Liu, Designing advanced S-scheme CdS QDs/La-Bi2WO6 photocatalysts for efficient degradation of RhB, Explorations 3 (2023) 20230050, https://doi.org/10.1002/EXP.20230050.
[95] A. Tufani, A. Qureshi, J.H. Niazi, Iron oxide nanoparticles based magnetic luminescent quantum dots (MQDs) synthesis and biomedical/biological applications: a review, Mater. Sci. Eng. C 118 (2021), https://doi.org/10.1016/j.msec.2020.111545.
[96] Y. Xu, X. Wang, W.L. Zhang, F. Lv, S. Guo, Recent progress in two-dimensional inorganic quantum dots, Chem. Soc. Rev. 47 (2018) 586–625, https://doi.org/10.1039/C7CS00500H.
[97] B. Chen, D. Li, F. Wang, InP quantum dots: synthesis and lighting applications, Small 16 (2020) 2002454, https://doi.org/10.1002/smll.202002454.
[98] A.B. Ganganboina, A.D. Chowdhury, I.M. Khoris, R.A. Doong, T.C. Li, T. Hara, F. Abe, T. Suzuki, E.Y. Park, Hollow magnetic-fluorescent nanoparticles for dual-modality virus detection, Biosens. Bioelectron. 170 (2020) 112680, https://doi.org/10.1016/j.bios.2020.112680.
[99] H.L. Xu, J.J. Yang, D.L. ZhuGe, M.T. Lin, Q.Y. Zhu, B.H. Jin, M.Q. Tong, B. X. Shen, J. Xiao, Y.Z. Zhao, Glioma-targeted delivery of a theranostic liposome integrated with quantum dots, superparamagnetic iron oxide, and cilengitide for dual-imaging guiding cancer surgery, Adv. Healthcare Mater. 7 (2018) e1701130, https://doi.org/10.1002/adhm.201701130.
[100] M. Zhu, G. Diao, Review on the progress in synthesis and application of magnetic carbon nanocomposites, Nanoscale 3 (2011) 2748–2767, https://doi.org/10.1039/c1nr10165j.
[101] J. Liu, R. Li, B. Yang, Carbon dots: a new type of carbon-based nanomaterial with wide applications, ACS Cent. Sci. 6 (2020) 2179–2195, https://doi.org/10.1021/acscentsci.0c01306.
[102] H. Lu, W. Li, H. Dong, M. Wei, Graphene quantum dots for optical bioimaging, Small 15 (2019) 1902136, https://doi.org/10.1002/smll.201902136.
[103] D.M. Kroupa, B.K. Hughes, E.M. Miller, D.T. Moore, N.C. Anderson, B. D. Chernomordik, A.J. Nozik, M.C. Beard, Synthesis and spectroscopy of silver-doped PbSe quantum dots, J. Am. Chem. Soc. 139 (2017) 10382–10394, https://doi.org/10.1021/jacs.7b04551.
[104] I.V. Martynenko, D. Kusic, F. Weigert, S. Stafford, F.C. Donnelly, R. Evstigneev, Y. Gromova, A.V. Baranov, B. Ruhle, H.J. Kunte, Y.K. Gun'ko, U. Resch-Genger, Magneto-fluorescent microbeads for bacteria detection constructed from superparamagnetic Fe3O4 nanoparticles and AIS/ZnS quantum dots, Anal. Chem. 91 (2019) 12661–12669, https://doi.org/10.1021/acs.analchem.9b01812.
[105] H.-Y. Liu, Z.-G. Wang, S.-L. Liu, D.-W. Pang, Single-virus tracking with quantum dots in live cells, Nat. Protoc. 18 (2023) 458–489, https://doi.org/10.1038/s41596-022-00775-7.
[106] X. Zhou, X. Zhang, S. Han, Y. Dou, M. Liu, L. Zhang, J. Guo, Q. Shi, G. Gong, R. Wang, J. Hu, X. Li, J. Zhang, Yeast microcapsule-mediated targeted delivery of diverse nanoparticles for imaging and therapy via the oral route, Nano Lett. 17 (2017) 1056–1064, https://doi.org/10.1021/acs.nanolett.6b04523.
[107] M.R. Shariati, A. Samadi-Maybodi, A.H. Colagar, Exploration of charge carrier delocalization in the iron oxide/CdS type-II heterojunction band alignment for enhanced solar-driven photocatalytic and antibacterial applications, J. Hazard Mater. 366 (2019) 475–481, https://doi.org/10.1016/j.jhazmat.2018.12.025.
[108] B. Das, A. Girigoswami, A. Dutta, P. Pal, J. Dutta, P. Dadhich, P.K. Srivas, S. Dhara, Carbon nanodots doped super-paramagnetic iron oxide nanoparticles for multimodal bioimaging and osteochondral tissue regeneration via external magnetic actuation, ACS Biomater. Sci. Eng. 5 (2019) 3549–3560, https://doi.org/10.1021/acsbiomaterials.9b00571.
[109] F. Wo, R. Xu, Y. Shao, Z. Zhang, M. Chu, D. Shi, S. Liu, A multimodal system with synergistic effects of magneto-mechanical, photothermal, photodynamic and chemo therapies of cancer in graphene-quantum dot-coated hollow magnetic nanospheres, Theranostics 6 (2016) 485–500, https://doi.org/10.7150/thno.13411.
[110] M. Thangamuthu, K.Y. Hsieh, P.V. Kumar, G.Y. Chen, Graphene- and graphene oxide-based nanocomposite platforms for electrochemical biosensing applications, Int. J. Mol. Sci. 20 (2019), https://doi.org/10.3390/ijms20122975.
[111] H. Zhang, H. Zhang, A. Aldalbahi, X. Zuo, C. Fan, X. Mi, Fluorescent biosensors enabled by graphene and graphene oxide, Biosens. Bioelectron. 89 (2017) 96–106, https://doi.org/10.1016/j.bios.2016.07.030.
[112] T. Lage, R.O. Rodrigues, S. Catarino, J. Gallo, M. Banobre-Lopez, G. Minas, Graphene-based magnetic nanoparticles for theranostics: an overview for their potential in clinical application, Nanomaterials 11 (2021), https://doi.org/10.3390/nano11051073.
[113] B. Du, J. Liu, G. Ding, X. Han, D. Li, E. Wang, J. Wang, Positively charged graphene/Fe3O4/polyethylenimine with enhanced drug loading and cellular uptake for magnetic resonance imaging and magnet-responsive cancer therapy, Nano Res. 10 (2017) 2280–2295, https://doi.org/10.1007/s12274-016-1418-x.
[114] T. Soltani, B.-K. Lee, Sono-synthesis of nanocrystallized BiFeO3/reduced graphene oxide composites for visible photocatalytic degradation improvement of bisphenol A, Chem. Eng. J. 306 (2016) 204–213, https://doi.org/10.1016/j.cej.2016.07.051.
[115] M. Aliabadi, H. Shagholani, A. Yunessnia Lehi, Synthesis of a novel biocompatible nanocomposite of graphene oxide and magnetic nanoparticles for drug delivery, Int. J. Biol. Macromol. 98 (2017) 287–291, https://doi.org/10.1016/j.ijbiomac.2017.02.012.
[116] K. Yang, L. Hu, X. Ma, S. Ye, L. Cheng, X. Shi, C. Li, Y. Li, Z. Liu, Multimodal imaging guided photothermal therapy using functionalized graphene nanosheets anchored with magnetic nanoparticles, Adv. Mater. 24 (2012) 1868–1872, https://doi.org/10.1002/adma.201104964.
[117] J. Xu, A. Gulzar, P. Yang, H. Bi, D. Yang, S. Gai, F. He, J. Lin, B. Xing, D. Jin, Recent advances in near-infrared emitting lanthanide-doped nanoconstructs: mechanism, design and application for bioimaging, Coord. Chem. Rev. 381 (2019) 104–134, https://doi.org/10.1016/j.ccr.2018.11.014.
[118] X. Wang, R.R. Valiev, T.Y. Ohulchanskyy, H. Ågren, C. Yang, G. Chen, Dye-sensitized lanthanide-doped upconversion nanoparticles, Chem. Soc. Rev. 46 (2017) 4150–4167, https://doi.org/10.1039/C7CS00053G.
[119] K. Xu, C. Lin, M.-F. Qin, Z. Yuan, Y. Tao, S.-S. Bao, R. Chen, X. Xie, L.-M. Zheng, Amplifying photoluminescence of lanthanide-doped nanoparticles by iridium phosphonate complex, ACS Mater. Lett. 5 (2023) 854–861, https://doi.org/10.1021/acsmaterialslett.2c01125.
[120] Q. Ma, J. Wang, Z. Li, X. Lv, L. Liang, Q. Yuan, Recent progress in time-resolved biosensing and bioimaging based on lanthanide-doped nanoparticles, Small 15 (2019) 1804969, https://doi.org/10.1002/smll.201804969.
[121] Y. Fan, L. Liu, F. Zhang, Exploiting lanthanide-doped upconversion nanoparticles with core/shell structures, Nano Today 25 (2019) 68–84, https://doi.org/10.1016/j.nantod.2019.02.009.
[122] A. Gnach, A. Bednarkiewicz, Lanthanide-doped up-converting nanoparticles: merits and challenges, Nano Today 7 (2012) 532–563, https://doi.org/10.1016/j.nantod.2012.10.006.
[123] A. Bagheri, H. Arandiyan, C. Boyer, M. Lim, Lanthanide-doped upconversion nanoparticles: emerging intelligent light-activated drug delivery systems, Adv. Sci. 3 (2016) 1500437, https://doi.org/10.1002/advs.201500437.
[124] H. Oliveira, A. Bednarkiewicz, A. Falk, E. Fröhlich, D. Lisjak, A. Prina-Mello, S. Resch, C. Schimpel, I.V. Vrček, E. Wysokińska, H.H. Gorris, Critical considerations on the clinical translation of upconversion nanoparticles (UCNPs): recommendations from the European upconversion network (COST action CM1403), Adv. Healthcare Mater. 8 (2019) 1801233, https://doi.org/10.1002/adhm.201801233.
[125] H. Chen, B. Ding, P.a. Ma, J. Lin, Recent progress in upconversion nanomaterials for emerging optical biological applications, Adv. Drug Deliv. Rev. 188 (2022) 114414, https://doi.org/10.1016/j.addr.2022.114414.
[126] Z. Wang, C. Liu, Y. Zhao, M. Hu, D. Ma, P. Zhang, Y. Xue, X. Li, Photomagnetic nanoparticles in dual-modality imaging and photo-sonodynamic activity against bacteria, Chem. Eng. J. 356 (2019) 811–818, https://doi.org/10.1016/j.cej.2018.09.077.
[127] Q. Fu, H. Feng, L. Liu, Z. Li, J. Li, J. Hu, C. Hu, X. Yan, H. Yang, J. Song, Spatiotemporally controlled formation and rotation of magnetic nanochains in vivo for precise mechanotherapy of tumors, Angew Chem. Int. Ed. Engl. 61 (2022) e202213319, https://doi.org/10.1002/anie.202213319.
[128] W.Q. Lim, Z. Gao, Plasmonic nanoparticles in biomedicine, Nano Today 11 (2016) 168–188, https://doi.org/10.1016/j.nantod.2016.02.002.
[129] J. Lim, S.A. Majetich, Composite magnetic–plasmonic nanoparticles for biomedicine: manipulation and imaging, Nano Today 8 (2013) 98–113, https://doi.org/10.1016/j.nantod.2012.12.010.
[130] S. Stafford, R. Serrano Garcia, Y. Gun'ko, Multimodal magnetic-plasmonic nanoparticles for biomedical applications, Appl. Sci. 8 (2018), https://doi.org/10.3390/app8010097.

[131] C. de la Encarnacion, D. Jimenez de Aberasturi, L.M. Liz-Marzan, Multifunctional plasmonic-magnetic nanoparticles for bioimaging and hyperthermia, Adv. Drug Deliv. Rev. 189 (2022) 114484, https://doi.org/10.1016/j.addr.2022.114484.
[132] P. Das, P. Fatehbasharzad, M. Colombo, L. Fiandra, D. Prosperi, Multifunctional magnetic gold nanomaterials for cancer, Trends Biotechnol. 37 (2019) 995–1010, https://doi.org/10.1016/j.tibtech.2019.02.005.
[133] M. Yuan, X. Feng, T.-H. Yan, J. Chen, X. Ma, P. Cunha, S. Lan, Y. Li, H.-C. Zhou, Y. Wang, Superparamagnetic iron oxide-enclosed hollow gold nanostructure with tunable surface plasmon resonances to promote near-infrared photothermal conversion, Adv. Compos. Hybrid Mater. 5 (2022) 2387–2398, https://doi.org/10.1007/s42114-022-00444-z.
[134] L. Hao, Y. Leng, L. Zeng, X. Chen, J. Chen, H. Duan, X. Huang, Y. Xiong, X. Chen, Core-shell-heterostructured magnetic-plasmonic nanoassemblies with highly retained magnetic-plasmonic activities for ultrasensitive bioanalysis in complex matrix, Adv. Sci. 7 (2020) 1902433, https://doi.org/10.1002/advs.201902433.
[135] E. Liu, M. Zhang, H. Cui, J. Gong, Y. Huang, J. Wang, Y. Cui, W. Dong, L. Sun, H. He, V.C. Yang, Tat-functionalized Ag-Fe(3)O(4) nano-composites as tissue-penetrating vehicles for tumor magnetic targeting and drug delivery, Acta Pharm. Sin. B 8 (2018) 956–968, https://doi.org/10.1016/j.apsb.2018.07.012.
[136] T. Du, G. Shi, F. Liu, T. Zhang, W. Chen, Sulfidation of Ag and ZnO nanomaterials significantly affects protein corona composition: implications for human exposure to environmentally aged nanomaterials, Environ. Sci. Technol. 53 (2019) 14296–14307, https://doi.org/10.1021/acs.est.9b04332.
[137] R. Das, N. Rinaldi-Montes, J. Alonso, Z. Amghouz, E. Garaio, J.A. Garcia, P. Gorria, J.A. Blanco, M.H. Phan, H. Srikanth, Boosted hyperthermia therapy by combined AC magnetic and photothermal exposures in Ag/Fe3O4 nanoflowers, ACS Appl. Mater. Interfaces 8 (2016) 25162–25169, https://doi.org/10.1021/acsami.6b09942.
[138] Y. Jiang, K. Pu, Molecular probes for autofluorescence-free optical imaging, Chem. Rev. 121 (2021) 13086–13131, https://doi.org/10.1021/acs.chemrev.1c00506.
[139] A.S. Klymchenko, F. Liu, M. Collot, N. Anton, Dye-loaded nanoemulsions: biomimetic fluorescent nanocarriers for bioimaging and nanomedicine, Adv. Healthcare Mater. 10 (2021) 2001289, https://doi.org/10.1002/adhm.202001289.
[140] Y. Liu, L. Teng, X.-F. Lou, X.-B. Zhang, G. Song, "Four-In-One" design of a hemicyanine-based modular scaffold for high-contrast activatable molecular afterglow imaging, J. Am. Chem. Soc. 145 (2023) 5134–5144, https://doi.org/10.1021/jacs.2c11466.
[141] Y. Ma, J. Shang, L. Liu, M. Li, X. Xu, H. Cao, L. Xu, W. Sun, G. Song, X.-B. Zhang, Rational design of a double-locked photoacoustic probe for precise in vivo imaging of cathepsin B in atherosclerotic plaques, J. Am. Chem. Soc. 145 (2023) 17881–17891, https://doi.org/10.1021/jacs.3c04981.
[142] L. Lei, F. Yang, X. Meng, L. Xu, P. Liang, Y. Ma, Z. Dong, Y. Wang, X.-B. Zhang, G. Song, Noninvasive imaging of tumor glycolysis and chemotherapeutic resistance via de novo design of molecular afterglow scaffold, J. Am. Chem. Soc. 145 (44) (2023) 24386–24400, https://doi.org/10.1021/jacs.3c09473.
[143] A.H. Ashoka, I.O. Aparin, A. Reisch, A.S. Klymchenko, Brightness of fluorescent organic nanomaterials, Chem. Soc. Rev. 52 (2023) 4525–4548, https://doi.org/10.1039/D2CS00464J.
[144] A. Reisch, A.S. Klymchenko, Fluorescent polymer nanoparticles based on dyes: seeking brighter tools for bioimaging, Small 12 (2016) 1968–1992, https://doi.org/10.1002/smll.201503396.
[145] Z. Lei, C. Sun, P. Pei, S. Wang, D. Li, X. Zhang, F. Zhang, Stable, wavelength-tunable fluorescent dyes in the NIR-II region for in vivo high-contrast bioimaging and multiplexed biosensing, Angew. Chem., Int. Ed. 58 (2019) 8166–8171, https://doi.org/10.1002/anie.201904182.
[146] K. Hola, Z. Markova, G. Zoppellaro, J. Tucek, R. Zboril, Tailored functionalization of iron oxide nanoparticles for MRI, drug delivery, magnetic separation and immobilization of biosubstances, Biotechnol. Adv. 33 (2015) 1162–1176, https://doi.org/10.1016/j.biotechadv.2015.02.003.
[147] Y. Sun, P. Sun, Z. Li, L. Qu, W. Guo, Natural flavylium-inspired far-red to NIR-II dyes and their applications as fluorescent probes for biomedical sensing, Chem. Soc. Rev. 51 (2022) 7170–7205, https://doi.org/10.1039/D2CS00179A.
[148] S. Lim, H.Y. Yoon, H.J. Jang, S. Song, W. Kim, J. Park, K.E. Lee, S. Jeon, S. Lee, D. K. Lim, B.S. Kim, D.E. Kim, K. Kim, Dual-modal imaging-guided precise tracking of bioorthogonally labeled mesenchymal stem cells in mouse brain stroke, ACS Nano 13 (2019) 10991–11007, https://doi.org/10.1021/acsnano.9b02173.
[149] S. Liu, Y. Jiang, P. Liu, Y. Yi, D. Hou, Y. Li, X. Liang, Y. Wang, Z. Li, J. He, H. Rong, D. Wang, J. Zhang, Single-atom gadolinium nano-contrast agents with high stability for tumor T1 magnetic resonance imaging, ACS Nano 17 (9) (2023) 8053–8063, https://doi.org/10.1021/acsnano.2c09664.
[150] Z. Wang, F. Carniato, Y. Xie, Y. Huang, Y. Li, S. He, N. Zang, J.D. Rinehart, M. Botta, N.C. Gianneschi, High relaxivity gadolinium-polydopamine nanoparticles, Small 13 (2017) 1701830, https://doi.org/10.1002/smll.201701830.
[151] H. Li, Y. Zeng, H. Zhang, Z. Gu, Q. Gong, K. Luo, Functional gadolinium-based nanoscale systems for cancer theranostics, J. Contr. Release 329 (2021) 482–512, https://doi.org/10.1016/j.jconrel.2020.08.064.
[152] Q. Meng, M. Wu, Z. Shang, Z. Zhang, R. Zhang, Responsive gadolinium(III) complex-based small molecule magnetic resonance imaging probes: design, mechanism and application, Coord. Chem. Rev. 457 (2022) 214398, https://doi.org/10.1016/j.ccr.2021.214398.
[153] H.-L. Wang, D. Liu, J.-H. Jia, J.-L. Liu, Z.-Y. Ruan, W. Deng, S. Yang, S.-G. Wu, M.-L. Tong, High-stability spherical lanthanide nanoclusters for magnetic resonance imaging, Natl. Sci. Rev. 10 (2023), https://doi.org/10.1093/nsr/nwad036.
[154] J. Chen, T. Chen, Q. Fang, C. Pan, O.U. Akakuru, W. Ren, J. Lin, A. Sheng, X. Ma, A. Wu, Gd2O3/b-TiO2 composite nanoprobes with ultra-high photoconversion efficiency for MR image-guided NIR-II photothermal therapy, Explorations 2 (2022) 20220014, https://doi.org/10.1002/EXP.20220014.
[155] S. Wang, J. Lin, Z. Wang, Z. Zhou, R. Bai, N. Lu, Y. Liu, X. Fu, O. Jacobson, W. Fan, J. Qu, S. Chen, T. Wang, P. Huang, X. Chen, Core–satellite polydopamine–gadolinium-metallofullerene nanotheranostics for multimodal imaging guided combination cancer therapy, Adv. Mater. 29 (2017) 1701013, https://doi.org/10.1002/adma.201701013.
[156] H. Chen, G.D. Wang, X. Sun, T. Todd, F. Zhang, J. Xie, B. Shen, Mesoporous silica as nanoreactors to prepare Gd-encapsulated carbon dots of controllable sizes and magnetic properties, Adv. Funct. Mater. 26 (2016) 3973–3982, https://doi.org/10.1002/adfm.201504177.
[157] Z. Wu, Z. Huang, G. Yin, L. Wang, F. Gao, Fabrication of Gd/Eu-codoped SmPO4 nanorods for dual-modal magnetic resonance and bio-optical imaging, J. Colloid Interface Sci. 466 (2016) 1–11, https://doi.org/10.1016/j.jcis.2015.10.048.
[158] W. Xu, H. Liu, D. Zhou, X. Chen, N. Ding, H. Song, H. Ågren, Localized surface plasmon resonances in self-doped copper chalcogenide binary nanocrystals and their emerging applications, Nano Today 33 (2020) 100892, https://doi.org/10.1016/j.nantod.2020.100892.
[159] I. Kriegel, C. Jiang, J. Rodríguez-Fernández, R.D. Schaller, D.V. Talapin, E. da Como, J. Feldmann, Tuning the excitonic and plasmonic properties of copper chalcogenide nanocrystals, J. Am. Chem. Soc. 134 (2012) 1583–1590, https://doi.org/10.1021/ja207798q.
[160] Z. Zhang, B. Chen, H. Xu, Z. Cui, S. Dong, A. Du, J. Ma, Q. Wang, X. Zhou, G. Cui, Self-established rapid magnesiation/de-magnesiation pathways in binary selenium–copper mixtures with significantly enhanced Mg-ion storage reversibility, Adv. Funct. Mater. 28 (2018) 1701718, https://doi.org/10.1002/adfm.201701718.
[161] C. Coughlan, M. Ibanez, O. Dobrozhan, A. Singh, A. Cabot, K.M. Ryan, Compound copper chalcogenide nanocrystals, Chem. Rev. 117 (2017) 5865–6109, https://doi.org/10.1021/acs.chemrev.6b00376.
[162] B. Yun, H. Zhu, J. Yuan, Q. Sun, Z. Li, Synthesis, modification and bioapplications of nanoscale copper chalcogenides, J. Mater. Chem. B 8 (2020) 4778–4812, https://doi.org/10.1039/d0tb00182a.
[163] W. Yang, W. Guo, W. Le, G. Lv, F. Zhang, L. Shi, X. Wang, J. Wang, S. Wang, J. Chang, B. Zhang, Albumin-bioinspired Gd:CuS nanotheranostic agent for in vivo photoacoustic/magnetic resonance imaging-guided tumor-targeted photothermal therapy, ACS Nano 10 (2016) 10245–10257, https://doi.org/10.1021/acsnano.6b05760.
[164] X. Jiang, S. Zhang, F. Ren, L. Chen, J. Zeng, M. Zhu, Z. Cheng, M. Gao, Z. Li, Ultrasmall magnetic CuFeSe(2) ternary nanocrystals for multimodal imaging guided photothermal therapy of cancer, ACS Nano 11 (2017) 5633–5645, https://doi.org/10.1021/acsnano.7b01032.
[165] D.E. Lee, H. Koo, I.C. Sun, J.H. Ryu, K. Kim, I.C. Kwon, Multifunctional nanoparticles for multimodal imaging and theragnosis, Chem. Soc. Rev. 41 (2012) 2656–2672, https://doi.org/10.1039/c2cs15261d.
[166] J. Kim, Y. Piao, T. Hyeon, Multifunctional nanostructured materials for multimodal imaging, and simultaneous imaging and therapy, Chem. Soc. Rev. 38 (2009) 372–390, https://doi.org/10.1039/b709883a.
[167] Z. Dong, P. Liang, G. Guan, B. Yin, Y. Wang, R. Yue, X. Zhang, G. Song, Overcoming hypoxia-induced ferroptosis resistance via a 19F/1H-MRI traceable core-shell nanostructure, Angew. Chem. Int. Ed. 61 (2022) e202206074, https://doi.org/10.1002/anie.202206074.
[168] J. Xu, G. Guan, Z. Ye, C. Zhang, Y. Guo, Y. Ma, C. Lu, L. Lei, X.B. Zhang, G. Song, Enhancing lipid peroxidation via radical chain transfer reaction for MRI guided and effective cancer therapy in mice, Sci. Bull. 68 (2023), https://doi.org/10.1016/j.scib.2023.12.036.
[169] L. Wang, Q. Wan, R. Zhang, B. Situ, K. Ni, J. Gao, X. Feng, P. Zhang, Z. Wang, A. Qin, B.Z. Tang, Synergistic enhancement of fluorescence and magnetic resonance signals assisted by albumin aggregate for dual-modal imaging, ACS Nano 15 (2021) 9924–9934, https://doi.org/10.1021/acsnano.1c01251.
[170] Z. Zhou, L. Yang, J. Gao, X. Chen, Structure–relaxivity relationships of magnetic nanoparticles for magnetic resonance imaging, Adv. Mater. 31 (2019) 1804567, https://doi.org/10.1002/adma.201804567.
[171] H.-W. Cheng, H.-Y. Tsao, C.-S. Chiang, S.-Y. Chen, Advances in magnetic nanoparticle-mediated cancer immune-theranostics, Adv. Healthcare Mater. 10 (2021) 2001451, https://doi.org/10.1002/adhm.202001451.
[172] G. Guan, C. Zhang, H. Liu, Y. Wang, Z. Dong, C. Lu, B. Nan, R. Yue, X. Yin, X. B. Zhang, G. Song, Ternary alloy PtWMn as a Mn nanoreservoir for high-field MRI monitoring and highly selective ferroptosis therapy, Angew. Chem., Int. Ed. Engl. 61 (2022) e202117229, https://doi.org/10.1002/anie.202117229.
[173] C. Zhang, L. Xu, B. Nan, C. Lu, H. Liu, L. Lei, R. Yue, G. Guan, M. He, X.B. Zhang, G. Song, Dynamic-reversible MRI nanoprobe for continuous imaging redox homeostasis in hepatic ischemia-reperfusion injury, ACS Nano 17 (2023) 9529–9542, https://doi.org/10.1021/acsnano.3c02265.
[174] H. Zhao, H. Zhao, Y. Jiao, Y. Zhu, C. Liu, F. Li, Y. Wang, Z. Gu, D. Yang, Biosynthetic molecular imaging probe for tumor-targeted dual-modal fluorescence/magnetic resonance imaging, Biomaterials 256 (2020) 120220, https://doi.org/10.1016/j.biomaterials.2020.120220.
[175] Y. Wang, Y. Hu, D. Ye, Activatable multimodal probes for in vivo imaging and theranostics, Angew Chem. Int. Ed. Engl. 61 (2022) e202209512, https://doi.org/10.1002/anie.202209512.
[176] R. Yan, Y. Hu, F. Liu, S. Wei, D. Fang, A.J. Shuhendler, H. Liu, H.Y. Chen, D. Ye, Activatable NIR fluorescence/MRI bimodal probes for in vivo imaging by enzyme-

mediated fluorogenic reaction and self-assembly, J. Am. Chem. Soc. 141 (2019) 10331–10341, https://doi.org/10.1021/jacs.9b03649.
[177] R. Yue, M. Zhou, X. Li, L. Xu, C. Lu, Z. Dong, L. Lei, H. Liu, G. Guan, Q. Liu, X.-B. Zhang, G. Song, GSH/APE1 cascade-activated nanoplatform for imaging therapy resistance dynamics and enzyme-mediated adaptive ferroptosis, ACS Nano 17 (14) (2023) 13792–13810, https://doi.org/10.1021/acsnano.3c03443.
[178] Q. Fu, R. Zhu, J. Song, H. Yang, X. Chen, Photoacoustic imaging: contrast agents and their biomedical applications, Adv. Mater. 31 (2019) e1805875, https://doi.org/10.1002/adma.201805875.
[179] R. Zhang, K. Cheng, A.L. Antaris, X. Ma, M. Yang, S. Ramakrishnan, G. Liu, A. Lu, H. Dai, M. Tian, Z. Cheng, Hybrid anisotropic nanostructures for dual-modal cancer imaging and image-guided chemo-thermo therapies, Biomaterials 103 (2016) 265–277, https://doi.org/10.1016/j.biomaterials.2016.06.063.
[180] Z. Chen, R. Chen, C. Zhao, Z. Quan, H. Zhu, L. Wang, Q. Bu, Y. He, H. He, A novel medically imageable intelligent cellulose nanofibril-based injectable hydrogel for the chemo-photothermal therapy of tumors, Chem. Eng. J. 431 (2022) 133255, https://doi.org/10.1016/j.cej.2021.133255.
[181] Y. Ma, W. Sun, Z. Ye, L. Liu, M. Li, J. Shang, X. Xu, H. Cao, L. Xu, Y. Liu, X. Kong, G. Song, X.B. Zhang, Oxidative stress biomarker triggered multiplexed tool for auxiliary diagnosis of atherosclerosis, Sci. Adv. 9 (2023), https://doi.org/10.1126/sciadv.adh1037 eadh1037.
[182] Y. Liu, X. Yang, Z. Huang, P. Huang, Y. Zhang, L. Deng, Z. Wang, Z. Zhou, Y. Liu, H. Kalish, N.M. Khachab, X. Chen, Z. Nie, Magneto-plasmonic Janus vesicles for magnetic field-enhanced photoacoustic and magnetic resonance imaging of tumors, Angew. Chem., Int. Ed. Engl. 55 (2016) 15297–15300, https://doi.org/10.1002/anie.201608338.
[183] Y. Duan, Y. Xu, D. Mao, W.H. Liew, B. Guo, S. Wang, X. Cai, N. Thakor, K. Yao, C. J. Zhang, B. Liu, Photoacoustic and magnetic resonance imaging bimodal contrast agent displaying amplified photoacoustic signal, Small 14 (2018) e1800652, https://doi.org/10.1002/smll.201800652.
[184] D. Yan, W. Xie, J. Zhang, L. Wang, D. Wang, B.Z. Tang, Donor/π-Bridge manipulation for constructing a stable NIR-II aggregation-induced emission luminogen with balanced phototheranostic performance, Angew. Chem. Int. Ed. 60 (2021) 26769–26776, https://doi.org/10.1002/anie.202111767.
[185] J. Zhao, J. Chen, S. Ma, Q. Liu, L. Huang, X. Chen, K. Lou, W. Wang, Recent developments in multimodality fluorescence imaging probes, Acta Pharm. Sin. B 8 (2018) 320–338, https://doi.org/10.1016/j.apsb.2018.03.010.
[186] Y. Liu, N. Kang, J. Lv, Z. Zhou, Q. Zhao, L. Ma, Z. Chen, L. Ren, L. Nie, Deep photoacoustic/luminescence/magnetic resonance multimodal imaging in living subjects using high-efficiency upconversion nanocomposites, Adv. Mater. 28 (2016) 6411–6419, https://doi.org/10.1002/adma.201506460.
[187] C. Lu, Z. Li, N. Wu, D. Lu, X.-B. Zhang, G. Song, Tumor microenvironment-tailored nanoplatform for companion diagnostic applications of precise cancer therapy, Chem 9 (2023) 3185–3211, https://doi.org/10.1016/j.chempr.2023.06.011.
[188] Y. Duan, M. Wu, D. Hu, Y. Pan, F. Hu, X. Liu, N.v. Thakor, W. Ng, X. Liu, Z. Sheng, H. Zheng, B. Liu, Biomimetic nanocomposites cloaked with bioorthogonally labeled glioblastoma cell membrane for targeted multimodal imaging of brain tumors, Adv. Funct. Mater. 30 (2020), https://doi.org/10.1002/adfm.202004346.
[189] H. Arami, A.P. Khandhar, A. Tomitaka, E. Yu, P.W. Goodwill, S.M. Conolly, K. M. Krishnan, In vivo multimodal magnetic particle imaging (MPI) with tailored magneto/optical contrast agents, Biomaterials 52 (2015) 251–261, https://doi.org/10.1016/j.biomaterials.2015.02.040.
[190] P. Ludewig, N. Gdaniec, J. Sedlacik, N.D. Forkert, P. Szwargulski, M. Graeser, G. Adam, M.G. Kaul, K.M. Krishnan, R.M. Ferguson, A.P. Khandhar, P. Walczak, J. Fiehler, G. Thomalla, C. Gerloff, T. Knopp, T. Magnus, Magnetic particle imaging for real-time perfusion imaging in acute stroke, ACS Nano 11 (2017) 10480–10488, https://doi.org/10.1021/acsnano.7b05784.
[191] Z.W. Tay, S. Savliwala, D.W. Hensley, K.L.B. Fung, C. Colson, B.D. Fellows, X. Zhou, Q. Huynh, Y. Lu, B. Zheng, P. Chandrasekharan, S.M. Rivera-Jimenez, C. M. Rinaldi-Ramos, S.M. Conolly, Superferromagnetic nanoparticles enable order-of-magnitude resolution & sensitivity gain in magnetic particle imaging, Small Methods 5 (2021) 2100796, https://doi.org/10.1002/smtd.202100796.
[192] C. Lu, L. Han, J. Wang, J. Wan, G. Song, J. Rao, Engineering of magnetic nanoparticles as magnetic particle imaging tracers, Chem. Soc. Rev. 50 (2021) 8102–8146, https://doi.org/10.1039/d0cs00260g.
[193] L. Meng, X. Ma, S. Jiang, G. Ji, W. Han, B. Xu, J. Tian, W. Tian, High-efficiency fluorescent and magnetic multimodal probe for long-term monitoring and deep penetration imaging of tumors, J. Mater. Chem. B 7 (2019) 5345–5351, https://doi.org/10.1039/c9tb00638a.
[194] G. Song, X. Zheng, Y. Wang, X. Xia, S. Chu, J. Rao, A magneto-optical nanoplatform for multimodality imaging of tumors in mice, ACS Nano 13 (2019) 7750–7758, https://doi.org/10.1021/acsnano.9b01436.
[195] J.W.M. Bulte, Superparamagnetic iron oxides as MPI tracers: a primer and review of early applications, Adv. Drug Deliv. Rev. 138 (2019) 293–301, https://doi.org/10.1016/j.addr.2018.12.007.
[196] P. Li, D. Wang, J. Hu, X. Yang, The role of imaging in targeted delivery of nanomedicine for cancer therapy, Adv. Drug Deliv. Rev. 189 (2022) 114447, https://doi.org/10.1016/j.addr.2022.114447.
[197] H. Huang, A. Ali, Y. Liu, H. Xie, S. Ullah, S. Roy, Z. Song, B. Guo, J. Xu, Advances in image-guided drug delivery for antibacterial therapy, Adv. Drug Deliv. Rev. 192 (2023) 114634, https://doi.org/10.1016/j.addr.2022.114634.
[198] L. Zhang, Y. Liu, H. Huang, H. Xie, B. Zhang, W. Xia, B. Guo, Multifunctional nanotheranostics for near infrared optical imaging-guided treatment of brain tumors, Adv. Drug Deliv. Rev. 190 (2022) 114536, https://doi.org/10.1016/j.addr.2022.114536.
[199] S. Liu, X. Pan, H. Liu, Two-dimensional nanomaterials for photothermal therapy, Angew. Chem. Int. Ed. 59 (2020) 5890–5900, https://doi.org/10.1002/anie.201911477.
[200] H.S. Jung, P. Verwilst, A. Sharma, J. Shin, J.L. Sessler, J.S. Kim, Organic molecule-based photothermal agents: an expanding photothermal therapy universe, Chem. Soc. Rev. 47 (2018) 2280–2297, https://doi.org/10.1039/C7CS00522A.
[201] Y. Yang, T. Yang, F. Chen, C. Zhang, B. Yin, X. Yin, L. Han, Q. Xie, X.B. Zhang, G. Song, Degradable magnetic nanoplatform with hydroxide ions triggered photoacoustic, MR imaging, and photothermal conversion for precise cancer theranostic, Nano Lett. 22 (2022) 3228–3235, https://doi.org/10.1021/acs.nanolett.1c04804.
[202] L. Wang, H. Lin, X. Chi, C. Sun, J. Huang, X. Tang, H. Chen, X. Luo, Z. Yin, J. Gao, A self-assembled biocompatible nanoplatform for multimodal MR/fluorescence imaging assisted photothermal therapy and prognosis analysis, Small 14 (2018) e1801612, https://doi.org/10.1002/smll.201801612.
[203] S. Li, W. Jiang, Y. Yuan, M. Sui, Y. Yang, L. Huang, L. Jiang, M. Liu, S. Chen, X. Zhou, Delicately designed cancer cell membrane-camouflaged nanoparticles for targeted 19F MR/PA/FL imaging-guided photothermal therapy, ACS Appl. Mater. Interfaces 12 (2020) 57290–57301, https://doi.org/10.1021/acsami.0c13865.
[204] Y. Pu, W. Wu, B. Zhou, H. Xiang, J. Yu, H. Yin, Y. Zhang, D. Du, Y. Chen, H. Xu, Starvation therapy enabled "switch-on" NIR-II photothermal nanoagent for synergistic in situ photothermal immunotherapy, Nano Today 44 (2022) 101461, https://doi.org/10.1016/j.nantod.2022.101461.
[205] R.-H. Deng, M.-Z. Zou, D. Zheng, S.-Y. Peng, W. Liu, X.-F. Bai, H.-S. Chen, Y. Sun, P.-H. Zhou, X.-Z. Zhang, Nanoparticles from cuttlefish ink inhibit tumor growth by synergizing immunotherapy and photothermal therapy, ACS Nano 13 (2019) 8618–8629, https://doi.org/10.1021/acsnano.9b02993.
[206] Q. Fu, Z. Li, J. Ye, Z. Li, F. Fu, S.L. Lin, C.A. Chang, H. Yang, J. Song, Magnetic targeted near-infrared II PA/MR imaging guided photothermal therapy to trigger cancer immunotherapy, Theranostics 10 (2020) 4997–5010, https://doi.org/10.7150/thno.43604.
[207] B. Sun, C. Luo, W. Cui, J. Sun, Z. He, Chemotherapy agent-unsaturated fatty acid prodrugs and prodrug-nanoplatforms for cancer chemotherapy, J. Contr. Release 264 (2017) 145–159, https://doi.org/10.1016/j.jconrel.2017.08.034.
[208] Q. Gao, J. Feng, W. Liu, C. Wen, Y. Wu, Q. Liao, L. Zou, X. Sui, T. Xie, J. Zhang, Y. Hu, Opportunities and challenges for co-delivery nanomedicines based on combination of phytochemicals with chemotherapeutic drugs in cancer treatment, Adv. Drug Deliv. Rev. 188 (2022) 114445, https://doi.org/10.1016/j.addr.2022.114445.
[209] W. Niu, Y. Guo, Y. Xue, M. Wang, M. Chen, D.D. Winston, W. Cheng, B. Lei, Biodegradable multifunctional bioactive Eu-Gd-Si-Ca glass nanoplatform for integrative imaging-targeted tumor therapy-recurrence inhibition-tissue repair, Nano Today 38 (2021), https://doi.org/10.1016/j.nantod.2021.101137.
[210] X. Sun, M. Zhang, R. Du, X. Zheng, C. Tang, Y. Wu, J. He, W. Huang, Y. Wang, Z. Zhang, X. Han, J. Qian, K. Zhong, X. Tian, L. Wu, G. Zhang, Z. Wu, D. Zou, A polyethyleneimine-driven self-assembled nanoplatform for fluorescence and MR dual-mode imaging guided cancer chemotherapy, Chem. Eng. J. 350 (2018) 69–78, https://doi.org/10.1016/j.cej.2018.05.157.
[211] S. Diao, Y. Liu, Z. Guo, Z. Xu, J. Shen, W. Zhou, C. Xie, Q. Fan, Prolonging treatment window of photodynamic therapy with self-amplified H2O2-activated photodynamic/chemo combination therapeutic nanomedicines, Adv. Healthcare Mater. 12 (2023) 2301732, https://doi.org/10.1002/adhm.202301732.
[212] Z. Li, Z. Zhou, Y. Wang, J. Wang, L. Zhou, H.-B. Cheng, J. Yoon, Activatable nano-photosensitizers for precise photodynamic cancer therapy, Coord. Chem. Rev. 493 (2023) 215324, https://doi.org/10.1016/j.ccr.2023.215324.
[213] D. Ni, C.A. Ferreira, T.E. Barnhart, V. Quach, B. Yu, D. Jiang, W. Wei, H. Liu, J. W. Engle, P. Hu, W. Cai, Magnetic targeting of nanotheranostics enhances cerenkov radiation-induced photodynamic therapy, J. Am. Chem. Soc. 140 (2018) 14971–14979, https://doi.org/10.1021/jacs.8b09374.
[214] C. Chen, C. Wu, J. Yu, X. Zhu, Y. Wu, J. Liu, Y. Zhang, Photodynamic-based combinatorial cancer therapy strategies: tuning the properties of nanoplatform according to oncotherapy needs, Coord. Chem. Rev. 461 (2022) 214495, https://doi.org/10.1016/j.ccr.2022.214495.
[215] X. Liang, M. Chen, P. Bhattarai, S. Hameed, Y. Tang, Z. Dai, Complementing cancer photodynamic therapy with ferroptosis through iron oxide loaded porphyrin-grafted lipid nanoparticles, ACS Nano 15 (2021) 20164–20180, https://doi.org/10.1021/acsnano.1c08108.
[216] B. Ji, M. Wei, B. Yang, Recent advances in nanomedicines for photodynamic therapy (PDT)-driven cancer immunotherapy, Theranostics 12 (2022) 434–458, https://doi.org/10.7150/thno.67300.
[217] G. Shu, W. Zhu, Y. Jiang, X. Li, J. Pan, X. Zhang, X. Zhang, S.-K. Sun, Persistent luminescence immune hydrogel for photodynamic-immunotherapy of tumors in vivo, Adv. Funct. Mater. 31 (2021) 2104472, https://doi.org/10.1002/adfm.202104472.
[218] R. Liang, L. Liu, H. He, Z. Chen, Z. Han, Z. Luo, Z. Wu, M. Zheng, Y. Ma, L. Cai, Oxygen-boosted immunogenic photodynamic therapy with gold nanocages@manganese dioxide to inhibit tumor growth and metastases, Biomaterials 177 (2018) 149–160, https://doi.org/10.1016/j.biomaterials.2018.05.051.
[219] N. Goswami, Z. Luo, X. Yuan, D.T. Leong, J. Xie, Engineering gold-based radiosensitizers for cancer radiotherapy, Mater. Horiz. 4 (2017) 817–831, https://doi.org/10.1039/C7MH00451F.
[220] Z. Zhang, X. Liu, D. Chen, J. Yu, Radiotherapy combined with immunotherapy: the dawn of cancer treatment, Signal Transduct. Targeted Ther. 7 (2022) 258, https://doi.org/10.1038/s41392-022-01102-y.

[221] D. De Ruysscher, G. Niedermann, N.G. Burnet, S. Siva, A.W.M. Lee, F. Hegi-Johnson, Radiotherapy toxicity, Nat. Rev. Dis. Prim. 5 (2019) 13, https://doi.org/10.1038/s41572-019-0064-5.
[222] W.J. Xiao, L. Zhao, Y. Sun, X. Yang, Q.R. Fu, Stimuli-responsive nanoradiosensitizers for enhanced cancer radiotherapy, Small Methods 7 (2023), https://doi.org/10.1002/smtd.202301131.
[223] M.Z. Wang, Q.R. Fu, Nanomaterials for disease treatment by modulating the pyroptosis pathway, Adv. Healthcare Mater. 12 (2023), https://doi.org/10.1002/adhm.202301266.
[224] J. Chen, C. Ning, Z. Zhou, P. Yu, Y. Zhu, G. Tan, C. Mao, Nanomaterials as photothermal therapeutic agents, Prog. Mater. Sci. 99 (2019) 1–26, https://doi.org/10.1016/j.pmatsci.2018.07.005.
[225] S. Lu, X. Li, J. Zhang, C. Peng, M. Shen, X. Shi, Dendrimer-stabilized gold nanoflowers embedded with ultrasmall iron oxide nanoparticles for multimode imaging-guided combination therapy of tumors, Adv. Sci. 5 (2018) 1801612, https://doi.org/10.1002/advs.201801612.
[226] M.-A. Shahbazi, L. Faghfouri, M.P.A. Ferreira, P. Figueiredo, H. Maleki, F. Sefat, J. Hirvonen, H.A. Santos, The versatile biomedical applications of bismuth-based nanoparticles and composites: therapeutic, diagnostic, biosensing, and regenerative properties, Chem. Soc. Rev. 49 (2020) 1253–1321, https://doi.org/10.1039/C9CS00283A.
[227] J. Xiao, L. Zeng, S. Ding, Y. Chen, X. Zhang, X.-w. Bian, G. Tian, Tumor-tropic adipose-derived mesenchymal stromal cell mediated Bi2Se3 nano-radiosensitizers delivery for targeted radiotherapy of non-small cell lung cancer, Adv. Healthcare Mater. 11 (2022) 2200143, https://doi.org/10.1002/adhm.202200143.
[228] Y. Li, Y. Sun, T. Cao, Q. Su, Z. Li, M. Huang, R. Ouyang, H. Chang, S. Zhang, Y. Miao, A cation-exchange controlled core-shell MnS@Bi(2)S(3) theranostic platform for multimodal imaging guided radiation therapy with hyperthermia boost, Nanoscale 9 (2017) 14364–14375, https://doi.org/10.1039/c7nr02384g.
[229] D. An, J. Fu, B. Zhang, N. Xie, G. Nie, H. Ågren, M. Qiu, H. Zhang, NIR-II responsive inorganic 2D nanomaterials for cancer photothermal therapy: recent advances and future challenges, Adv. Funct. Mater. 31 (2021) 2101625, https://doi.org/10.1002/adfm.202101625.
[230] P. Tang, Y. Liu, Y. Liu, H. Meng, Z. Liu, K. Li, D. Wu, Thermochromism-induced temperature self-regulation and alternating photothermal nanohelix clusters for synergistic tumor chemo/photothermal therapy, Biomaterials 188 (2019) 12–23, https://doi.org/10.1016/j.biomaterials.2018.10.008.
[231] H. Guo, S. Yi, K. Feng, Y. Xia, X. Qu, F. Wan, L. Chen, C. Zhang, In situ formation of metal organic framework onto gold nanorods/mesoporous silica with functional integration for targeted theranostics, Chem. Eng. J. 403 (2021), https://doi.org/10.1016/j.cej.2020.126432.
[232] L. Huang, L. Ao, D. Hu, W. Wang, Z. Sheng, W. Su, Magneto-plasmonic nanocapsules for multimodal-imaging and magnetically guided combination cancer therapy, Chem. Mater. 28 (2016) 5896–5904, https://doi.org/10.1021/acs.chemmater.6b02413.